Lawrence Berkeley National Laboratory
LBL Publications

Title
Techno-economic perspective on emerging cryogenic and non-cryogenic boil-off hydrogen compression systems

Permalink
https://escholarship.org/uc/item/1w34v22r

Journal
Applied Energy, 427

ISSN
0306-2619

Authors
Banerjee, Tanumoy
Xhafa, Ingrid
Witman, Matthew D
et al.

Publication Date
2027

DOI
10.1016/j.apenergy.2026.129146

Copyright Information
This work is made available under the terms of a Creative Commons Attribution-NonCommercial-NoDerivatives License, available at https://creativecommons.org/licenses/by-nc-nd/4.0/

Peer reviewed

eScholarship.org Powered by the California Digital Library
University of California

Techno-economic perspective on emerging cryogenic and non-cryogenic boil-off hydrogen compression systems

Tanumoy Banerjee [a], Ingrid Xhafa [a], Matthew Witman [b], Cullen Quine [c], Sarah Shulda [c], Thomas Gennett [c, d], Hanna Breunig [a, *]

[a] Energy Analysis Division, Lawrence Berkeley National Laboratory, Berkeley, California 94704, USA

[b] Sandia National Laboratories, Livermore, California 94550, USA

[c] Hydrogen Systems and Technologies Advanced Research Group, National Laboratory of the Rockies, Golden, Colorado 80401, USA

[d] Department of Chemistry, Colorado School of Mines, Golden, Colorado 80401, USA

*Correspondence: hannabreunig@lbl.gov, 1 Cyclotron Road, 90-2012, Berkeley, CA 94720

Abstract: Boil-off hydrogen (BOH) loss from liquid hydrogen (LH_2) storage and transfer infrastructure poses a critical challenge to the use of hydrogen in emerging aviation, space, and heavy-duty mobility applications. As LH_2 infrastructure expands, it becomes paramount to identify strategies to minimize BOH loss, enhance exergy efficiency, and reduce safety risks associated with hydrogen leakage. This work presents a detailed techno-economic comparison of BOH management, including novel process designs for 5-8 tonnes per day high flow rate BOH recovery and compression up to 700 bar, from BOH at 2 bar, 60 K. Compression systems include a thermally integrated three-stage mechanical compressor-intercooler, a cryogenic re-liquefaction-vaporization cryo-pump, and four best-in-class metal hydride (MH)-based chemical compressors, with and without thermal integration. The re-liquefaction-vaporization pathway (<$3/kg-BOH at 90% cumulative probability for 350 bar) reduces compression cost by 31% compared with best-in-class MH systems (reduction of 19% and 30% for 100 bar and 700 bar). Mechanical compression systems are the most expensive, however all compression systems look favorable compared with venting of BOH at current market prices for LH_2.

Keywords: *Liquid hydrogen, Boil-off hydrogen, Techno-economic analysis, Metal hydride, Mechanical compression*

1. Introduction:

Among different hydrogen storage technologies, physical storage in either compressed gas form (ranging from 170 to 700 bar tanks) or liquid hydrogen (LH_2) form (at cryogenic temperature of ~ -253 °C) is well established. Due to the high densities offered by LH_2 for bulk storage and transport, the space sector has long relied on cryogenic storage. Given the current high price of LH_2 and concerns related to the direct emission of H_2, the prevention or capture of boil-off hydrogen (BOH) has received increased attention from industry and the scientific community [1–3]. Boil-off occurs due to a number of processes that drive instability in the temperature and pressure of the liquefied H_2. Well-known examples include drops in volumetric density (i.e., reduction in mass of hydrogen per unit volume due to temperature rise or *ortho–para* conversion (spin isomers of hydrogen) causing thermal expansion and reduced liquid density), continuous heat ingress, temperature mismatch between LH_2 and system components, two-phase flow instabilities, intermittent dispensing, sloshing during transport, and flashing during transfer or refueling events [2]. Boil-off is released at pressures around 3-6 bar and temperatures around -243 °C or higher [4,5], with a distinctly high *para*-to-*ortho* ratio.[2,6] Loss of LH_2 to boil-off is estimated at 0.1-0.3% per day from storage tanks [2], and at 2-20% from transport or refueling transfers [7]. While insulation can reduce BOH during long-duration storage, reducing BOH during transfer events remains a challenge despite recent thermodynamic approaches for improvements at flow rates relevant to vehicle refueling [1].

Reducing the occurrence of BOH is an ambitious objective, and in the interim, there is value in capturing the BOH for subsequent use. One barrier facing the utilization of BOH as a compressed gas product is the lack of physical models representing the operation requirements of BOH pressurization for subsequent use. Injection into pipelines or gaseous storage will require pressurization of the BOH between 100 and 700 bar. Incumbent mechanical compressors are inefficient at very low suction pressures, including high energy consumption and capital cost, noisy operation, and a deeper coolant loop to balance the thermal loads [8,9]. We address this gap by presenting novel process models, based on experimental data and thermodynamic physical modeling, for mechanical and chemical compression systems with and without cryogenic equipment.

The primary motivation of this work derives from the absence of process designs, and a unified process integration and techno-economic analysis (TEA) framework, of BOH compression strategies under the flow rates and operational conditions expected during airplane (on the order of 5-8 metric tonnes per day: tpd) refueling, derived through correspondences with Airbus. We address this research gap by presenting three novel BOH compression strategies—mechanical compression, metal-hydride-based thermally driven chemical compression, and re-liquefaction leveraging a cryopump–vaporization system similar to that proposed by Plug Power. This study quantifies the levelized cost of hydrogen compression (LCOH) across a range of discharge pressures (up to 700 bar) and explores the influence of hydride properties, energy prices, capacity factor, annual BOH throughput, and plant lifetime through sensitivity analyses. This comprehensive comparative framework allows us to identify the dominant cost drivers in each pathway, evaluate technological trade-offs, and establish the operating domains in which mechanical, MH-based, or re-liquefaction–driven BOH recovery becomes economically favorable. Understanding how these systems perform relative to one another is critical for guiding both technology development and infrastructure deployment.

1.1 Background:

Metal hydrides (MH) have emerged as an alternative compression technology that eliminates the need for mechanical moving parts by leveraging temperature-dependent equilibrium pressures for hydrogen absorption–desorption cycles. Hydrides have been studied for decades as hydrogen storage materials and are commonly classified into families based on composition and bonding characteristics (e.g., AB, AB_2, AB_5 intermetallic, complex). TiFe-based AB-type intermetallics have gained attention for their use of earth-abundant materials, and for demonstrating cyclability (>3000 cycles), with use by several companies for hydrogen storage [10–14]. MgH_2 may also offer low raw material cost, with high theoretical capacity (>5 wt.%), and scalability; however, its intrinsic cyclability in the bulk state is limited by slow hydrogen diffusion, surface oxidation, high thermodynamic stability (ΔH ~ 75 kJ/mol), which necessitates much higher desorption temperatures (>300 °C), and structural degradation during repeated hydriding/dehydriding cycles. Importantly, recent studies have shown that through nanostructuring, engineering the structure and chemistry by incorporating catalysts, and composites, Mg-based systems can achieve enhanced

reversibility and stable cycling performance, highlighting that cyclability is not an inherent property of bulk MgH_2 but rather dependent on the design of the material [15,16]. With regards to compression systems, AB, AB_2, and AB_5 intermetallic compounds offer favorable pressure-composition-temperature (PCT) characteristics which can be matched to the pressure targets of each compression stage. [27]

When considering MH for compression, experimental studies have demonstrated the feasibility of using AB_2 and AB_5 intermetallic hydrides for hydrogen compression at 700-865 bar (for AB_2) [11,12,17] and ~200 bar (for AB_5) [18]. Among them, AB_2 MHs are known to have higher reversible hydrogen storage capacity, faster release kinetics, wider and tunable plateau pressure, the ability to reach higher discharge pressures, while also relying on relatively lower raw material costs compared to AB_5 and complex hydrides [12,19,20]. $LaNi_5$ and Ti-based AB_2 hydrides offer stable cycling to achieve moderate (< 100 bar for $LaNi_5$) to high compression pressures (700-850 bar for Ti-Zr-Mn hydrides) at temperatures below 150 °C [12,21], whereas Mg-based alloys require much higher desorption temperatures (>275-350 °C) [22,23]. Accordingly, Ti-based AB_2 hydrides are selected for this study due to their suitability for achieving the targeted 350–700 bar pressure range at moderate operating temperatures.

Practically, MH compression is quieter in operation, has fewer failure point components,[24] and can be configured to handle intermittent gas flow, making them attractive for handling the intermittent production of BOH during LH_2 transfer scenarios. However, the broader techno-economic analysis of MH-compression systems remains uncertain due to limited data on hydride kinetics and reversible capacity, material costs, cycle life, and thermal management requirements. A challenge for MH development is that optimal operating temperatures, governed by hydride's thermodynamics and kinetics of hydrogen absorption, are highly material-dependent, and for many candidate hydrides, lie below those typical of H_2 streams produced directly from steam methane reforming or electrolysis (over 20-25 °C). Low-temperature inflows (e.g., -40 °C boil-off hydrogen) could thus enable efficient MH compression[25]. Herein, we present process designs for leveraging MH to compress BOH up to 700 bar with a -40 °C to 80 °C temperature swing. While most prior work has focused on materials performance and pressure amplification, the literature is absent of efforts toward system-level integration or comparative techno-economic analysis (TEA)

across compression technologies or MH under consistent duty conditions, leaving a critical gap in assessing MH compressors for industrial BOH scenarios.

Parallel to these approaches, re-liquefaction at cryogenic conditions followed by liquid-phase cryo-pumping represents an alternative pathway in which BOH is first condensed back to liquid and subsequently gets converted to high-pressure compressed hydrogen using a combination of positive-displacement cryogenic pumps and ambient vaporizers [26]. Since liquid phase pump work is much smaller than the energy required in high-pressure vapor-phase mechanical compression of BOH (because liquid hydrogen has a much smaller specific volume than gaseous hydrogen), this route has the potential to drastically reduce energy consumption compared to gas-phase compression. Recent developments in small-scale cryocoolers, mixed-refrigerant cryogenic cycles, and high-pressure cryopumps have demonstrated promising efficiency and cost improvements [27,28], with companies such as Plug Power and Verne leading the demonstration of cryopumping [29,30]. Upon correspondence with industry partners, we determined that a comprehensive TEA comparison between cryogenic and non-cryogenic low-temperature H_2 compression is a timely contribution.

2. Methods:

Process models are developed in the ASPEN Plus software [31–33] which has been widely used in process optimization and economics applied to hydrogen compression, liquefaction, and hydrogen energy storage systems [6,33–35]. Details of the system designs, process models, and cost analyses are provided in the following sections for 350 bar and 700 bar BOH compression systems. Parameter sensitivity and Monte Carlo analysis based on 50,000 simulations are performed to understand key drivers of performance and the likelihood of LCOH based on parameter distributions, and to explore scenario-aware outcomes such as unfavorable conditions or advances in material development.

All models assume that BOH enters the capture system at -213 °C (60 K), 2 bar. Equipment is sized to reflect a base case nameplate capacity capture rate of 5 tpd, which equates to 1825 tonnes per year (tpy) annual throughput at a capacity factor (CF) of 100%. This nameplate was selected to

represent the instantaneous BOH capture rate during a transfer/refueling event (based on our correspondence with industry partners like Airbus and Stoke Space Technologies), and should not be equated with steady state boil-off rate or a standing LH_2 inventory. Here, the CF is defined as the number of days the plant is actively capturing BOH in a calendar year, i.e., the number of full-flow operating days per year, so that the nameplate capacity of 1,825 tpy corresponds to 5 tpd at 100% CF. Under this definition, the low-CF (<100%) values essentially capture the realistic intermittent BOH capture scenario for transfer events, whereas the high-CF region represents an upper bound corresponding to a continuous transfer/refueling BOH capture, such as a co-located liquefaction facility at a large airport. In the sensitivity analysis, equipment was resized up to 8 tpd to capture annual throughput greater than 1,825 tpy.

2.1 Mechanical Compression System Design: We developed a multi-stage thermally-integrated compressor-intercooler system, as illustrated in **Figure 1**. Our system comprises three compression stages where the discharge pressures of the 1st, 2nd, and 3rd stages of compressors (Comp1, Comp2, and Comp3) are 11, 60, and 350 bar, respectively. Each compression stage is followed by a water-cooled intercooler that reduces the discharge temperature to approximately 27 °C, maintaining near-isothermal compression conditions and lowering the overall specific compression work [36,37]. Water at ambient conditions (20 °C) is employed as the cooling fluid in all three intercoolers. To enhance the compression efficiency, the temperature of BOH is elevated to 27 °C upstream of the first-stage compressor, using a part of the thermal energy recovered after the final compression stage (Comp3), as shown by the 'Heat Ex1b' block and represented by the red-dotted line in **Figure 1**. The thermodynamic performance of each compressor stage is evaluated using polytropic efficiency correlations and real-gas properties for hydrogen [37,38]. Pressure drops across intercoolers and connecting pipelines are assumed to be negligible (<1%), corresponding to the stage pressure [39,40]. This assumption is further justified by the large stage pressure ratios (11/2, 60/11, and 350/60), for which typical exchanger and piping pressure losses represent only a small fraction of the overall compression requirement. The final product stream is compressed gaseous hydrogen at 350 bar, which can be stored in high-pressure tanks for further utilization. The state point conditions for compressing BOH in this system at 350 bar are given in **Table S1** in the

electronic supplementary information (ESI). This integrated design provides substantial reductions in external heat demand and compression work relative to a non-integrated baseline system.

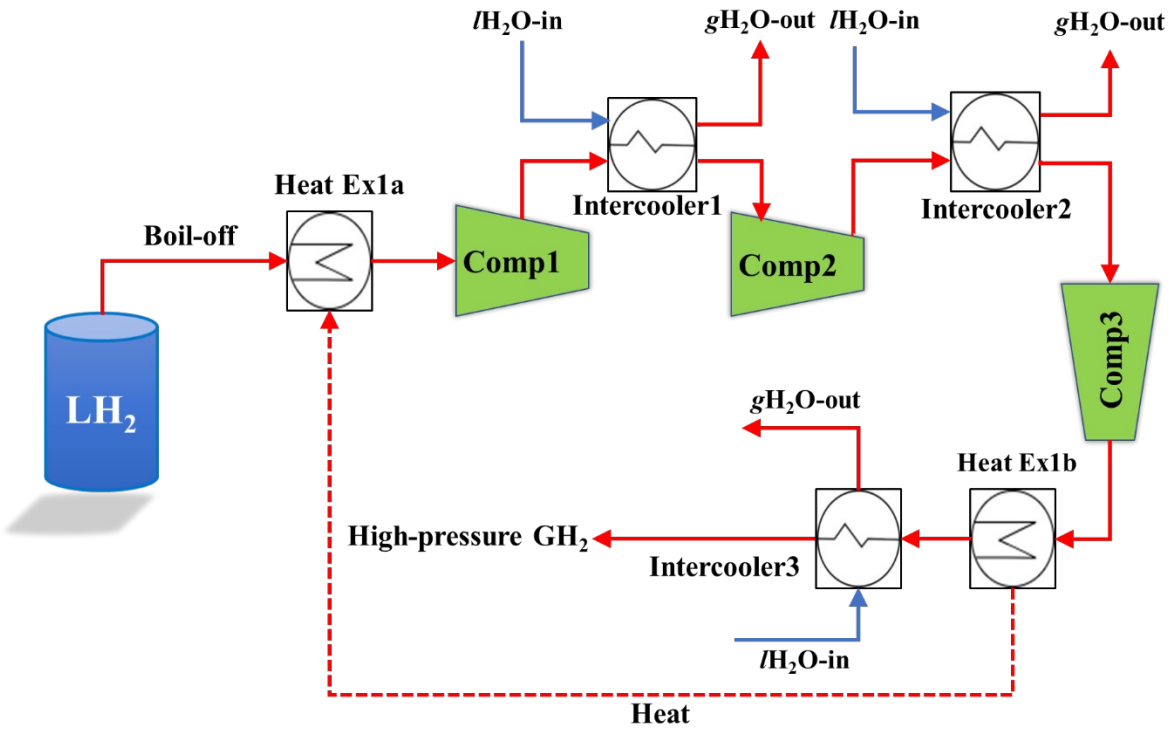


Figure 1. Schematic of the system and the key processes involved during multi-stage BOH compression using mechanical compressors. A part of the compression heat is used to raise the temperature of incoming BOH (in Heat Ex1a) to reduce the net heat load of the system. LH_2: liquid H_2; GH_2: gaseous H_2; *l*: liquid; *g*: gas; comp: compressor.

2.2 Re-liquefaction-Vaporization System Design: The re-liquefaction–vaporization-based BOH recovery system represents a highly integrated cryogenic process designed to maximize thermodynamic efficiency with reduced capital intensity. In this design, BOH first passes through a pre-cooling and re-condensation sequence rather than a conventional multi-stage gas compressor. The BOH feed is first precooled by indirect heat exchange with the returning cold liquid hydrogen stream exiting the downstream cryogenic section. This step primarily recovers internal cold energy and reduces the external refrigeration demand. In the subsequent precooling stage, the BOH stream is cooled against liquid helium (*l*-He) in a pre-cooler heat exchanger, lowering its temperature further from the initial boil-off condition (-213 °C) to about -233 °C (~40 K). This *l*-He-based pre-

cooling step removes the majority of sensible and latent heat from the BOH stream, ensuring that only a small residual refrigeration load must be handled by the cryocooler. After pre-cooling, the BOH stream is pressurized at 20 bar before the final cryogenic treatment. Subsequent refrigeration is provided by a cryocooler coupled with a catalytic *ortho*-to-*para* hydrogen (*o*-*p*H_2) conversion reactor located at the lowest temperature region of the cold box. This catalytic conversion drives the residual *o*-H_2 fraction in BOH to equilibrium *p*-H_2 within the reactor, where the associated exothermic heat is released together with the sensible and latent cooling duty by the cryocooler at that stage. This stabilizes the hydrogen phase and prevents self-heating and vapor regeneration of already condensed liquid hydrogen downstream. For the initial BOH feed at 60 K, 2 bar, we assumed the feed stream comprises of 20% *o*-H_2 and rest 80% *p*-H_2 [5,6]. The *o*-*p* conversion reactor not only enhances the thermodynamic stability of the condensed hydrogen but also reduces the cryocooler load by internalizing exothermic heat release. While the *o*-*p* conversion heat itself is a part of the cryocooler duty, the *p*-H_2-enriched BOH feed keeps the duty small and prevents any uncontrolled conversion, and all this heat duty is retained to calculate the necessary electrical shaft power used to compute the specific energy consumption of the system. The resulting high-purity LH_2 (at 100% *p*-H_2) can be routed back to LH_2 storage, or in this study, we assume it is routed to a cryogenic liquid pump.

The cryogenic liquid pump, comprising two positive-displacement (PD) stages (for 350 bar compression) and an intercooler to lower thermal load, pressurizes the LH_2 directly to high pressure (>300 bar) with minimal energy input. The compression work gets reduced significantly due to the high density and low compressibility of the liquid phase because liquid pumping work scales approximately with $\Delta P/\rho$ (rather than with $P.\ln\left(\frac{P_2}{P_1}\right)$ in gas compression). Cryopumps typically consume ~10-20% of the required energy of an equivalent mechanical gas compressor (~5-10× lower shaft power) [41]. The pressurized LH_2 enters a vaporizer, where thermal energy can be used to convert it to gaseous hydrogen at dispensing conditions. This re-liquefaction-vaporization design leverages available low-grade heat (ambient air, facility cooling-water return, or intercooler waste heat) to further minimize the utility demand. Heat rejected from the intercooler between the cryo-pump stages is reintegrated upstream in the pre-cooling section, creating a closed

thermal loop that eliminates the requirements of any external refrigeration systems. The system additionally avoids high-temperature reactors and cycling-induced thermal stresses inherent to MH compressors, enabling higher reliability than MH-based compression systems. State point conditions for this system are given in **Table S2**.

2.3 Metal Hydride System Design: The MH-based hydrogen compression system is designed to effectively compress BOH using a two-stage process that incorporates two parallel compressor trains (as denoted by two half-cycles), where the MH bed reactor is modeled as a custom block. In this block, the reaction enthalpy during absorption and desorption phases is accounted for. BOH enters the system, where it is first preheated and transferred through a heat exchanger (HX1) to reach -40 °C. The hydrogen at -40 °C then enters the first low-pressure compression stages operating simultaneously in parallel (Comp-1LP, and Comp-2LP) packed with MH, where it is compressed to 30 bar, with heat being added to facilitate the endothermic desorption of hydrogen from the MH beds. After the desorption from these two low-pressure compressors, hydrogen at 30 bar and 80 °C enters the hot side of the integrated intercooler, which uses compression heat (from 80 °C to -10 °C) to preheat the oncoming BOH, thereby eliminating the need for an external refrigeration unit and reducing energy demand effectively [25]. The subsequent high-pressure compression (HP Comp) stage, packed with MH, raises the hydrogen pressure further to 350 bar. This parallel system works in a way that when Comp-1LP is absorbing hydrogen downstream of the heat exchanger (HX1), Comp-2LP is simultaneously desorbing H_2 at 30 bar, and *vice versa* for high-pressure MH compressor beds, as we mentioned in one of our recent works [25]. This non-refrigerated novel integration strategy leverages synchronized hydrogenation and dehydrogenation cycles across multiple hydride beds in each stage, allowing for continuous operation and higher throughput [24,25]. While the process model could in theory be used to evaluate any class of MH, the selection of MH remains critical.

In our base case, we employed Ti-Zr-Cr-based AB_2-type hydride (from $Ti_{2-z}Zr_zCrMnFeNi$ family, with z=0.2-0.4) for compression up to 350 bar (**Figure 2**), for their favorable desorption kinetics. Achieving high-pressure desorption from MgH_2 requires significantly higher thermal energy compared to lower-enthalpy hydrides, and as such MgH_2 is only included as an option for 100 bar compression [23–25]. Additionally, for comparison under low-pressure, low-temperature absorption

conditions, a 350-bar hybrid MH case is considered that employs two distinct MHs in each of the two compression stages: Hydralloy C5 for the low-pressure stage[42] and a Ti–Zr–Cr–based AB_2 [10,25] for the high-pressure stage. For the first compression stage, the relevant design criterion is that the hydride must absorb BOH coming at the cold-end condition (~-40 °C, 2 bar). Hydralloy C5 satisfies this low-pressure requirement more naturally, with a reported mid-plateau absorption pressure of ~1.5 bar at -30 °C, whereas the $Ti_{2-z}Zr_zCrMnFeNi$ family exhibits substantially higher plateau pressures for z=0.2-0.4 [43]. For 700 bar applications discussed in Section 3.7, two different Ti–Zr–Cr–based AB_2 MH is applied, given their demonstrated ability to store hydrogen at high plateau pressures of up to 800 bar [25]. An effective thermal management system, incorporating internal heat exchangers and intercoolers, is essential to regulate the temperature swings required for hydrogen absorption and desorption, which strongly influences the system's efficiency and cycle time [44]. This approach enables the system to achieve high compression ratios with reduced temperature swings compared to single-stage compressors, improving energy efficiency and reducing operational costs. Overall, the integration of feasible heat management, optimized hydride materials, and synchronized cycling strategies is central to the development and performance of MH-based hydrogen compression systems [44,45].

We note that the MH compression performance reported here is a prospective, model-based system where the results are constructed using the experimentally measured MH properties: pressure–composition–temperature (PCT) isotherms, reversible/usable capacity of hydrogen at operating pressure ranges, plateau pressures, desorption enthalpies, and reported cycle-life ranges, combined with steady-state mass and energy balances for a two-bed half-cycle configuration (proposed in a previous study from our group [25], as per **Figure 2**). The competitive advantage of MH-based systems is contingent on the underlying material and kinetic assumptions. For our analysis, based on the designed assumption of a 5 tpd BOH capture rate and a nameplate capture capacity of 1,825 tpy, we have theoretically calculated the MH requirements in each case based on their PCT curves and related thermodynamic and operating conditions (**Table S3**). Additionally, we also note that transient desorption kinetics, thermal coupling, and achievable absorption-desorption cycle times remain the major sources of uncertainty and would require a dynamic, multi-bed prototype rather

than the quasi-dynamic system we designed for this study. We also identify experimental validation of the integrated dynamic compressor as a necessary direction for future work.

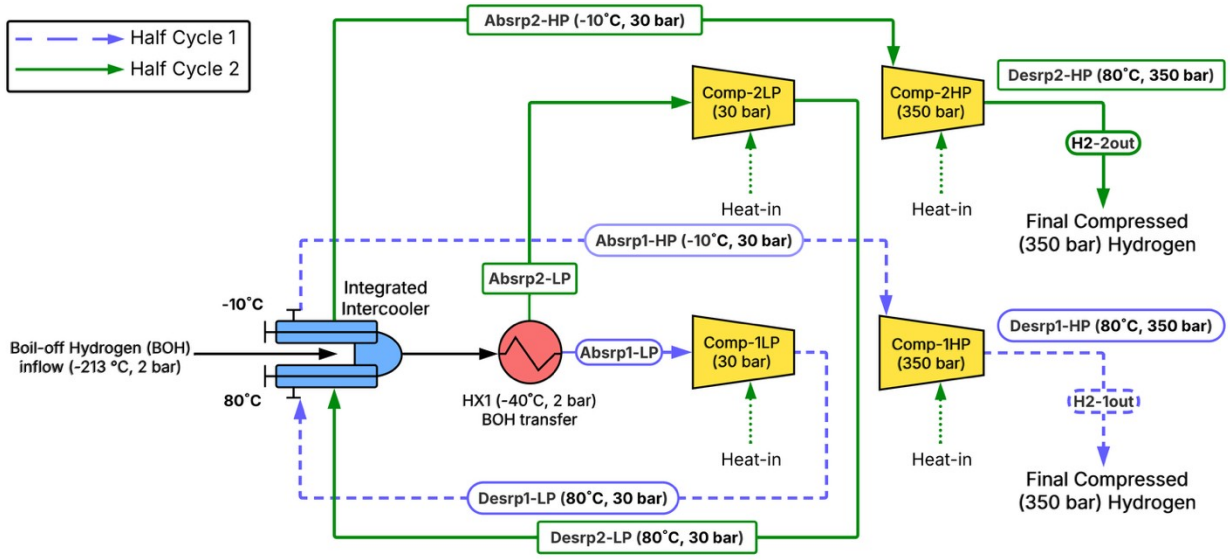


Figure 2. Schematic of the 2-stage MH-based hydrogen compression system with integrated thermal management. The intercooler is working as a heat exchanger (HX) to increase the temperature of the incoming BOH, utilizing the compression heat after the low-pressure compression (LP Comp) stage at 30 bar. In the hybrid system (section 3.3(b)), and 700 bar compression system (section 3.7), the LP and HP are packed with different types of MH materials. In the scenario of with a refrigeration loop (section 3.3(a)), there is no integrated intercooler, so the heat rejected by the LP compressor during desorption is taken away by the evaporator of the refrigeration cycle.

2.4 Cost and Uncertainty Analysis Methodology: The economic analysis is based on 2024 economic data. The LCOH is evaluated over an assumed plant operational period of 30 years with a capital expenditure period of three years (33 years total). The total overnight cost is assumed to be 100% depreciable over 20 years at a 150% declining balance [46,47]. After-tax weighted average cost of capital for an investor-owned utility with 55% debt financing is 4.73% (real) [46,47]. Tax rates are 21% (federal) and 6% (state) [46,47]. This financing structure results in a capital charge factor (CCF) of 0.0710. LCOH is determined using equation (1), and LCOH here represents the cost of capturing, compressing, and storing BOH in the first year, calculated by considering factors like the capital charge factor (CCF), the total cost of building the facility (TOC), fixed and variable annual operating costs (OC_{fix} and OC_{var}), the plant's utilization capacity factor (CF), and the expected annual quantity of BOH being captured and stored at full capacity, i.e., annual capacity (AC).

$$LCOH = \frac{(CCF * TOC + OC_{fix} + OC_{var.})}{(CF * AC)} \; where \; AC \neq 0 \quad (1)$$

The TOC is the total overnight capital expenditure, and it includes the total plant cost (TPC) as well as pre-production costs, inventory capital, financing costs, land, and other owners' costs [47,48]. The capital cost for the plant is estimated by identifying all major components incorporated into purchased equipment cost (EC) and assigning cost values and scaled cost either based on vendor data, literature, cost correlations, ASPEN Process Economic Analyzer (APEA) and then updating them to the reference year (in this case 2024) using the Chemical Engineering Plant Cost Index (CEPCI) [33,39,49–52]. The scaled cost (SC) is determined by using the reference cost (RC), annual escalation rate (AER), scaled year (SY), and respective reference year (RY). In order to scale the equipment size, the scaling parameter (SP), and the reference parameter (RP) at reference scale are used along with the scaling exponent (u), found in literature for different sets of plant-based major equipment. Additionally, an exponent of 0.9 is used to account for cost reduction when multiple units of the same equipment are purchased and installed. For the analysis, all costs are escalated to the year 2024 using an annual escalation rate of 3%. Finally, the scaling cost (SC) to the relevant analysis year is achieved by equation (2-3).

$$SC = RC.(1 + AER)^{SY - RY} \quad (2)$$

$$SC = RC.\left(\frac{SP}{RP}\right)^{u} * \left(\frac{TS}{TR}\right)^{0.9} \quad (3)$$

Fixed operating costs (OC_{fix}) include property tax and insurance at 2% of the TPC and operating labor. Operating labor for the BOH compression-storage facility at the relevant scale is estimated at 100% CF, with skilled operators paid at an hourly rate of $38.50, based on the median salary for power plant operators. It is estimated that the labor burden accounts for 30% of the operating costs, and an additional 25% will be allocated for overhead expenses. Maintenance costs are assumed to be around 3–5% of installed capital per year. Maintenance-related labor expenses are assumed to account for 30-40% of total maintenance costs, while maintenance materials contribute the remaining, and administrative and support labor are 25% of the combined operating and maintenance labor costs [39,47,48,53]. Operators per shift are derived from Turton [39].

Variable operating costs (OC_{var}), such as maintenance expenses, are dependent on the operation hours of the plant. OC_{var} includes items like fuel (electricity at \$300/MWh), cooling water (\$3/tonne), liquid helium (\$15/liter)[54], and catalysts that are consumed. We assume an iron-based oxide, commercially known as IONEX[35,55] catalyst at \$2.19/kg, with a lifetime of approximately 2 years for the *o*-H_2 to *p*-H_2 conversion during liquefaction, based on import data on Zauba. Experimental and plant-scale data for hydrous IONEX catalysts show no measurable loss in activity over at least five months of continuous operation (processing ~100,000 L of liquid) and repeated thermal cycling [56]. Given that the present system processes *para*-enriched (20% *p*-H_2) BOH, resulting in significantly lower conversion duty, catalyst degradation is expected to be dominated by contamination rather than intrinsic activity loss. Therefore, a 2-year catalyst lifetime is adopted as a conservative yet realistic assumption for techno-economic analysis. For the mechanical system, single or multi-stage diaphragm or piston-type compressor intercooler setups are designed and sized based on the BOH flow rate and operating conditions. For the MH-based system, the major components included MH reactors (containing materials like MgH_2, Hydralloy C5, and AB_2-type Ti-Zr-Cr hydrides), heat exchangers, intercoolers, flow control systems, and safety valves. The cost of MH is estimated based on raw material prices, a gross profit margin, and an estimate of energy costs necessary to manufacture the MH. In this work, the raw material cost for production is taken from available online resources and listed in **Table S4**, and utility pricing is added in order to reflect realistic manufacturing expenses in accordance with the methodology used in the techno-economic analysis presented in by Nandiyanto *et al.* [57]. In addition, the gross profit margin (GPM) is added to the final MH cost following the same ratio and calculation approach reported in the earlier study to quantify profitability relative to sales and cost of MH sold. From this, we find MgH_2 cost is estimated at \$25–35/kg, and other AB_2 hydrides used for the current analysis are within \$40–80/kg [57,58]. Our correspondence with alloy manufacturers of a titanium-based MH suggests these values are conservative. The equipment cost of heat exchangers in the compression and re-liquefaction-vaporizer system is estimated using standard literature correlations for shell-and-tube and cryogenic plate-fin units, following established methods from Turton et al. [39] and recent cost models reported in Shamoushaki et al. [59] (2021), along with liquefaction capital expenditure benchmarks from DOE H2A. [60]

Balance of plant (BOP) costs—including piping, electrical wiring, instrumentation, and insulation—are estimated as a fraction of the equipment cost, typically adding 50–70% of the total major equipment costs [64,65]. Installation and construction costs are estimated at 25–40% of equipment cost, depending on system complexity [64]. A Lang factor (f_L) of 2.5–3.0 is applied for packaged systems and 3.5–4.5 for field-installed units to estimate the total installed capital cost [66].

The total fixed capital cost (C_{cap}) for the system is calculated using *Equation (4)*,

$$C_{cap} = C_{equip} . \left(1 + f_{BOP} + f_{install}\right) \times f_L \quad (4)$$

where $0.5 < f_{BOP} < 0.7$; and $0.25 < f_{install} < 0.40$.

For MH systems, electricity consumption is primarily associated with heating (resistive or waste heat augmented) and control systems, whereas for mechanical systems, compression work is the main source of electricity demand. Material replacement costs for MH systems are modeled based on representative hydride degradation and replacement cycle frequency, with lifetimes ranging between 2,000 and 10,000 cycles [67,68].

Key variables identified through the previously described sensitivity analysis are further evaluated in both deterministic and probabilistic uncertainty analyses. A deterministic uncertainty analysis is used to explore the combined effect of practical near-term system and material improvements on levelized cost and total plant cost. Considerations such as setback space footprint and safety costs are not considered. Monte Carlo uncertainty quantification in which all economically influential parameters are varied simultaneously is performed to conduct a probabilistic uncertainty analysis. We sampled 50,000 trials spanning parameter distributions reflected in the deterministic uncertainty analysis: annual throughput of BOH (600–1,825 tpy), plant operating life (10-40 years), installation and balance-of-plant (BOP) factors (0.7–1.3× and 0.45–1.15×), and electricity price (0.4–2.5×base case), together with the MH-specific hydride material cost ($20–80/kg), cycle life (1000–10,000 cycles), and usable H_2 uptake (1.0–2.0 wt.%), and liquid helium price for the re-liquefaction-vaporization system ($5–40/L). Because a single deployment site imposes a common economic environment across all pathways, each of these cost drivers (throughput, plant life,

installation, BOP, material and electricity prices) is drawn once per trial and applied to all three systems, so that the analysis can give us a robust ranking.

3. Results and Discussion:

3.1 Low-Pressure Mechanical Compression: Mechanical compression up to 350 bar at 5 tpd nameplate and 100% CF consumes 5.86 GWh of electricity annually, corresponding to 89 % of the electric load. This corresponds to a specific energy consumption (SEC) of 3.21 kWh(e)/kg-H_2 compressed. Commercial data of compressing hydrogen at 350-360 bar indicate SEC of ~4.2-7.5 kWh(e)/kg-H_2 for large compressors, with some multi-stage systems reaching 8.3–11.2 kWh(e)/kg-H_2, [37] and this goes to 4.9 kWh(e)/kg-H_2 when compressing from 1 bar, 27 °C to 350 bar. In this study, the lower SEC is obtained mostly due to thermally integrated inter-stage heat recovery and the preheating of BOH feed (**Figure 1**), as well as the favorable inlet conditions of BOH compared to ambient-temperature hydrogen. The LCOH is estimated at \$5.12 /kg-H_2, with overnight capital cost responsible for 48% (\$2.48 /kg-H_2) and driving associated fixed operating costs at 27% (\$1.36 /kg-H_2) (**Figure S1a**). The TPC of \$28.5 million itself contributes \$2.03 /kg-H_2, highlighting the capital-intensive nature of conventional mechanical compressors. Concepts for optimizing the CAPEX by making compact compressor configurations, a modular system, and lowering hardware costs associated with auxiliary cooling systems and safety infrastructure could be opportunities for cost reduction, but are not explored further in this analysis. Among variable operating costs, maintenance materials (\$0.52 /kg-H_2) and cooling water demand for intercoolers (\$0.54 /kg-H_2) constitute the largest shares, whereas electricity required for compressor operation (\$0.23 /kg-H_2) is relatively low and moderately sensitive to the price of electricity, assumed to be 300 \$/MWh (**Figure S1c**).

At 5 tpd nameplate capacity, LCOH drops significantly when used 100 or more days per year (or more than 27% CF) to increase annual throughput. The LCOH decreases sharply from \$17.8 /kg-H_2 at 250 tonnes per yr (50 days) to ~\$3.5-4.0 /kg-H_2 at 1500–1800 tpy (300-360 days), which reflects improved utilization of initial higher CAPEX and lower per-unit operating expenditures

(**Figure S1b**). Interestingly, when the system's operational lifetime is shortened to 10 years, the LCOH increases by ~50% to \$7.84 /kg-H_2, which reflects the fact that a 10-year project period does not provide sufficient time to recover the overnight capital expenses incurred. Overall, the analysis highlights that scale, energy price, operational years, and operational-spare train combinations (depending on operational need and duty requirement for continuous runtime) are the primary levers controlling the economic performance of mechanical BOH compression systems (**Figure S1c**). Neither energy demand nor process efficiency scale strongly with a higher nameplate capacity of 8 tpd.

3.2 Low-Pressure Cryogenic Compression: For the re-liquefaction-vaporization pathway (**Figure 3a**), liquefaction and cryogenic pumping dominate electricity consumption, requiring approximately 1.74 GWh of electricity annually, corresponding to an SEC of 0.95 kWh(e)/kg-H_2 compressed. The SEC here includes the electricity required for (a) the He-precooler shaft work, (b) cryocooler shaft work rejecting the residual sensible, latent, and *o-p*H_2 conversion heat, (c) the 2→20 bar compressor work, and (d) the multi-stage cryogenic pump work. **Table S5** decomposes this 0.95 kWh(e)/kg-H_2 into the pre-cooler, cryocooler, compressor, cryogenic pump, and auxiliary duties. When used for re-liquefaction, rather than coupled with cryo-pumps for compression, we find the proposed system can re-liquefaction BOH for \$1.83 /kg-H_2. When this re-liquefaction loop is integrated with the liquid PD-pump-based pressure rise and vaporization train to achieve 350 bar gaseous H_2 product, the LCOH goes up to \$2.51 /kg-H_2, as shown in the cost distribution plot (**Figure 3b**). Overnight capital accounts for roughly 47% of total LCOH (~\$1.18 /kg-H_2), dominated by the cold-box equipment and cryogenic PD pump systems, and associated fixed operating costs are proportionally high. We note that we may be overestimating operating and administrative labor since these tasks are likely to be shared with existing LH_2 storage operations. Catalyst costs (here, iron-based oxide is used, IONEX[35,55]) for *o-p*H_2 conversion are negligible, whereas liquid helium purchase represents 6% of the total cost.

Similar to mechanical compression, the LCOH is strongly influenced by CF or annual plant throughput required to pay off fixed equipment capital costs (**Figure 3c and 3d**). Increasing throughput beyond 500 tpy makes this system more cost competitive compared to mechanical compression; however, LCOH begins to flatten at ~1,200–1,500 tpy, corresponding to ~240–300

operating days (capacity factor ≈ 65–80%). When considering drivers of costs (**Figure 3d**), it is worth noting that several parameters could compound to an unfavorable cost point for this technology. Specifically, re-liquefaction efficiency, liquid helium and electricity costs could occur simultaneously. Re-liquefaction efficiency defines the fraction of BOH that condensed back to liquid per cycle/pass (can also be termed as re-condensation ratio or BOH recovery fraction). Re-liquefaction efficiency is one of the critical factors for this system since it is necessary that only liquid hydrogen enters the pump-vaporizer system. Reducing re-liquefaction efficiency from 100% to 80% increases LCOH by ~\$0.50 /kg-H_2, reflecting the high penalty of increased *l*-He pre-cooler and cryocooler load. Overall, the results indicate that scaling, cold-end efficiency, and cryogenic utility pricing dominate the cost structure, and optimizing these levers is essential for minimizing the LCOH of the integrated re-liquefaction–vaporization system.

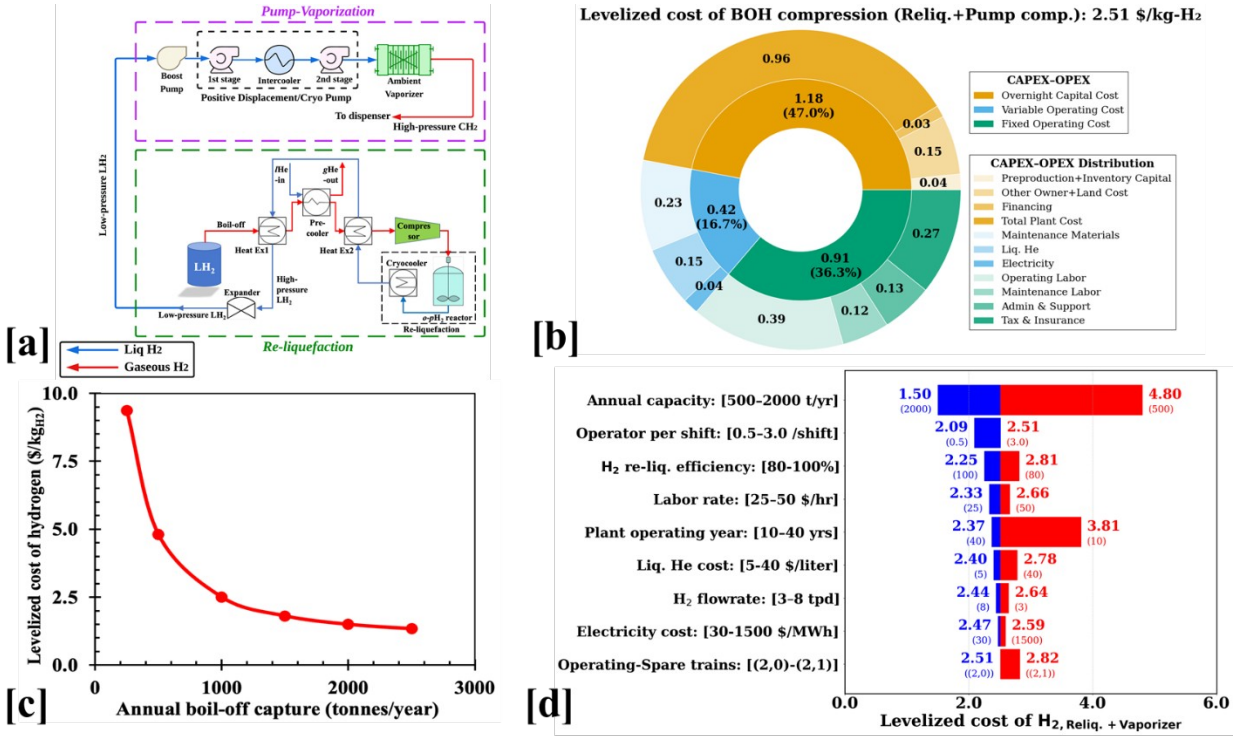


Figure 3. Integrated re-liquefaction and cryogenic liquid-pump 350 bar compression system for BOH recovery and techno-economic cost distribution; (a) schematic of the re-liquefaction–vaporizer based BOH compression configuration, where BOH is re-condensed using *l*-He and cryocooler-assisted heat exchangers, then pressurized in the liquid phase and vaporized to high-pressure compressed hydrogen (CH for dispensing, (b) Techno-economic breakdown showing a levelized cost of \$2.51 /kg-H_2, (c) Effect of annual BOH capture rate on the levelized cost this system, (d) Sensitivity results of the integrated system

showing the impact of key technical and economic parameter ranges provided in parenthesis on levelized cost of BOH capture.

3.3 Low-Pressure Metal Hydride Compression: The base case MH system uses $Ti_{2-x}Zr_xCrMnFeNi$-based MH ($Ti_{1.6}Zr_{0.4}CrMnFeNi$) in two stages without using BOH as a refrigeration loop. The system was evaluated with BOH as a means of system cooling, but this configuration was not cost effective. For this MH, we assume a working reversible H_2 capacity of 1.5 wt.% at 350 bar [25,69]. The material cost of $Ti_{1.6}Zr_{0.4}CrMnFeNi$ MH is estimated at $38/kg, which incorporates the raw elemental, energy cost, and GPM. A second design uses a hybrid MH system which employs Hydralloy C5 ($Ti_{0.95}Zr_{0.05}Mn_{1.46}V_{0.45}Fe_{0.09}$) estimated at $52/kg for 1st stage compression at 1.3 wt.% at 30 bar [43,70] and $Ti_{1.6}Zr_{0.4}CrMnFeNi$ for 2nd stage for compression at 350 bar. For low-pressure (100 bar) BOH compression, we present a system using MgH_2 estimated at $30/kg at 5.2 wt.% at 100 bar. The absorption and desorption pressure-temperature ranges, and temperature swings per stage are included in **Table S3** for the three proposed low-pressure MH compression configurations. The best-performing system for 350 bar (reflected in the base case) is subsequently modeled for 700 bar, as described in Section 3.7. The high-pressure system uses $Ti_{1.8}Zr_{0.2}CrMnFeNi$ in the 2nd stage compression to improve thermodynamic performance.

(a) Base case: The $Ti_{1.6}Zr_{0.4}CrMnFeNi$-based 350 bar compression system requires 11.72 GWh of thermal energy (corresponding to a SEC of 6.42 kWh(th)/kg-H_2 compressed) and 34 tonnes of MH per compression stage annually. We find the system achieves a LCOH 29% lower ($3.65 /kg-$H_2$) than mechanical compression and lowers TPC by half to $12.5 million. The cost of MH contributes to 38% of the LCOH, assuming ~2,000 absorption–desorption cycles, which we model as a variable operating expense (**Figure S2a**). Increasing system cycling beyond 200 days per year (1000 tonnes/year) plays a critical role in determining cost competitiveness (**Figure S2b**). Increasing the nameplate capacity to 8 tpd, has the lowest impact on increasing LCOH, suggesting some flexibility in sizing, so long as the MH recycle rate is held constant (**Figure S2c**). Other than the annual BOH capture capacity, the material cost, durability, recyclability, and hydrogen storage capacity (1–2 wt.%) drive system viability. When considering MH compression with a refrigeration system that uses the BOH, instead of the integrated intercooler (refer to **Figure 2**), the refrigeration system lowers the temperature of hydrogen after the first (LP) compression stage. The

integration of refrigeration-assisted heat management enhances hydrogen desorption rates; however, due to higher capital and fixed operating costs, the overall LCOH increases compared to the non-refrigeration case ($3.65 vs 4.14 /kg-$H_2$ shown in **Figure 4**), thereby offsetting efficiency gains.

(b) Hybrid MH: At 350 bar compression, a hybrid MH system leveraging two different MH requires 33 tonnes of Hydralloy and 42 tonnes of $Ti_{1.6}Zr_{0.4}CrMnFeNi$ for the first and second compression stages, respectively, which means the LP and HP compressors in **Figure 2** consist of two different MH beds. A total of 12.9 GWh thermal energy is required annually, leading to a SEC of 7.07 kWh(th)/kg-H_2 compressed. This hybrid system still demonstrates improved compression performance than the mechanical compression up to 350 bar but shows a >13% increase in LCOH compared to the $Ti_{1.6}Zr_{0.4}CrMnFeNi$-based MH compression system ($3.65 vs 4.13 /kg-$H_2$ shown in **Figure 4**). This increment can be attributed to the high material cost (vanadium at ~15% in molar ratio) and lower capacity of Hydralloy. However, if the H_2 storage capacity of Hydralloy increases to 1.4 wt.% and the material cost goes down to $30/kg, LCOH becomes equal to that of the $Ti_{1.6}Zr_{0.4}CrMnFeNi$-based MH case (i.e., $3.65 /kg-$H_2$). For such hybrid configurations, the MH material cost alone contributes up to 45% of the total LCOH, underscoring the significance of material cost and Hydrogen uptake capacity. The hybrid MH system provides the same LCOH as the non-hybrid with refrigeration scenario.

(c) MgH_2 compression system: Based on a desorption enthalpy of 74.7 kJ/mol-H_2 at a temperature of 524°C, for compression to 100 bar, a MgH_2 system requires 43.7 tonnes of MgH_2 and 19.01 GWh of thermal energy (SEC: 10.42 kWh(th)/kg-H_2 compressed) annually. At lower discharge pressure (100 bar), mechanical compression exhibits an LCOH of $3.24/kg-$H_2$, comprised of approximately 41% ($1.33/kg-$H_2$) in overnight capital cost. Under the same 100 bar discharge conditions, MgH_2-based compression achieves a lower LCOH of $2.73/kg-$H_2$ (assuming ~800 absorption-desorption cycles before replacement), reflecting reduced capital intensity and lower electricity demand relative to mechanical compression. This further underscores the competitiveness of MH-based compression even for low-pressure BOH recovery applications. As seen in **Figure 4**, compression to 100 bar, potentially suitable for injection into a local pipeline, leads to notably lower costs than 350 bar systems, and the MH selection should be considered

based on the final pressure target. In **Table 1**, we have summarized all the system parameters, thermodynamic hydrogen desorption capacity within the assumed pressure ranges of different MHs and the requirement of each of the MHs in each case.

Because the MH pathway is driven by thermal energy while the mechanical and re-liquefaction pathways are driven by electricity, the SEC values are not directly comparable on a raw kWh basis; the two energy carriers differ in both thermodynamic quality and economic value. Three complementary bases can be used for better comparison. (i) Economic basis: the levelized cost of hydrogen (LCOH) already internalizes these differences by pricing electricity at $300/MWh for the mechanical and re-liquefaction-vaporization pathways and treating MH desorption heat as low-grade heat. (ii) Primary-energy basis: applying the representative grid conversion efficiency and primary energy factor (PEF) value of 2.7 for the USA [71], the thermal SEC values for the mechanical and re-liquefaction-vaporization pathways correspond to 8.7 kWh (th)/kg-H_2 (since mechanical compression SEC is 3.21 kWh(e)/kg-H_2) and 2.6 kWh (th)/kg-H_2 (since re-liquefaction-vaporization system's SEC is, 0.95 kWh(e)/kg-H_2) respectively, whereas the base case AB_2 MH system's thermal SEC is 6.42 kWh(th)/kg-H_2. (iii) Exergy basis: electricity is essentially pure exergy (quality factor ≈ 1), while the thermal exergy associated with the desorption heat requirement for the MH system is based on its Carnot temperature factor and is dependent on the desorption temperatures given in **Table S3** (base case $Ti_{1.6}Zr_{0.4}CrMnFeNi$ desorbing at 80 °C in both stages); therefore, the 6.42 kWh(th)/kg-H_2 MH duty carries ~1.1 kWh-exergy/kg-H_2, comparable to the electrical input of re-liquefaction-vaporization (0.95kWh(e)/kg-H_2), and well below mechanical compression.

Table 1. Thermodynamic and system parameters, no. of compression stages of different MHs used in this study along with the specific energy consumption (SEC) for each case.

Parameter	**$Ti_{1.6}Zr_{0.4}CrMnFeNi$ (non-hybrid, 350 bar)**	**Hybrid: Hydralloy C5 (Stage 1) + $Ti_{1.6}Zr_{0.4}CrMnFeNi$ (Stage 2), 350 bar**	**$Ti_{1.6}Zr_{0.4}CrMnFeNi$ (Stage 1) + $Ti_{1.8}Zr_{0.4}CrMnFeNi$ (Stage 2), 700 bar**	**MgH_2 (100 bar)**
Reversible H_2 capacity within pressure	1.5 wt.% at 350 bar (sensitivity range 1–2 wt.%) [25,69].	Hydralloy: 1.3 wt.% at 30 bar; $Ti_{1.6}Zr_{0.4}CrMnFeNi$:	Stage 1: 1.5 wt.%; Stage 2: 1.2 wt.% (effective working	5.2 wt.% (desorption enthalpy 74.7 kJ/mol-

window		1.5 wt.%. [43,70].	capacity) [25].	H_2) [15, 23].
Desorption plateau pressure window	2→30 bar → 350 bar (2 stages)	Hydralloy: 2–30 bar (LP); $Ti_{1.6}Zr_{0.4}CrMnFeNi$: 30 to 350 bar (HP)	$Ti_{1.6}Zr_{0.4}CrMnFeNi$: 2–30 bar; $Ti_{1.8}Zr_{0.2}CrMnFeNi$: 30–700 bar	Desorption at 524 °C for 100 bar
Number of beds	2 stages (LP and HP compressor); refrigeration variant uses external refrigeration	2 different MH beds (LP and HP)	2 stages	Single stage
Number of cycles	~2,000 absorption–desorption cycles	~2,000 absorption–desorption cycles	~2,000 absorption–desorption cycles	~800 absorption–desorption cycles
Hydride mass required	34 tonnes per stage/year	33 tonnes Hydralloy (Stage 1) + 42 tonnes $Ti_{1.6}Zr_{0.4}CrMnFeNi$ (Stage 2)	34 tonnes (Stage 1) + 42.5 tonnes (Stage 2) per year	43.7 tonnes/year
Thermal energy / SEC	11.72 GWh; 6.42 kWh(th)/kg-H_2	12.9 GWh; 7.07 kWh(th)/kg-H_2	16.48 GWh; 9.03 kWh(th)/kg-H_2	19.01 GWh; 10.42 kWh(th)/kg-H_2

3.4 Low-Pressure BOH Compression Comparison: At 350 bar, the re-liquefaction-vaporization system emerges as the cheapest, most scalable solution with high confidence (**Figure 4, 5 and S3**), while MH compression offers the widest range in possible future costs resulting from variations in market, system, and material performance. The LCOH for $Ti_{1.6}Zr_{0.4}$CrMnFeNi-based MH systems ranges between \$2.51 to \$ 5.73/kg-H_2, whereas mechanical compression can go up to \$7.75/kg-H_2 (**Figure 4**). The 350 bar re-liquefaction-vaporization system consistently yields the lowest TPC (\$15.5–\$6.5M) and LCOH (\$3.04–\$1.32 /kg-H_2) at 100% CF due to several factors. First, liquid-phase pumping requires an order of magnitude less energy than gas-phase compression. and avoids hydride cost and associated material degradation entirely. Second, the cost advantage of 31% over the best-performing MH at 350 bar is primarily attained by the simplified equipment train, smaller footprint, and elimination of MH material cycling and degradation, all of which contribute to continuous and steady operation of BOH capture with lower maintenance overhead. Across the resulting LCOH distributions (**Figure S3**), the re-liquefaction-vaporization pathway remains the lowest-cost option in 96.2% of trials and is always cheaper than mechanical compression (100% of trials), while the complete cost ordering (re-liquefaction-vaporization < MH < mechanical) is preserved in 92.8% of the Monte Carlo trials. The only reversal in technology prioritization occurs when favorable MH material and thermodynamic parameters (low material cost, long cycle life, and high uptake) coincide with an unfavorable helium price.

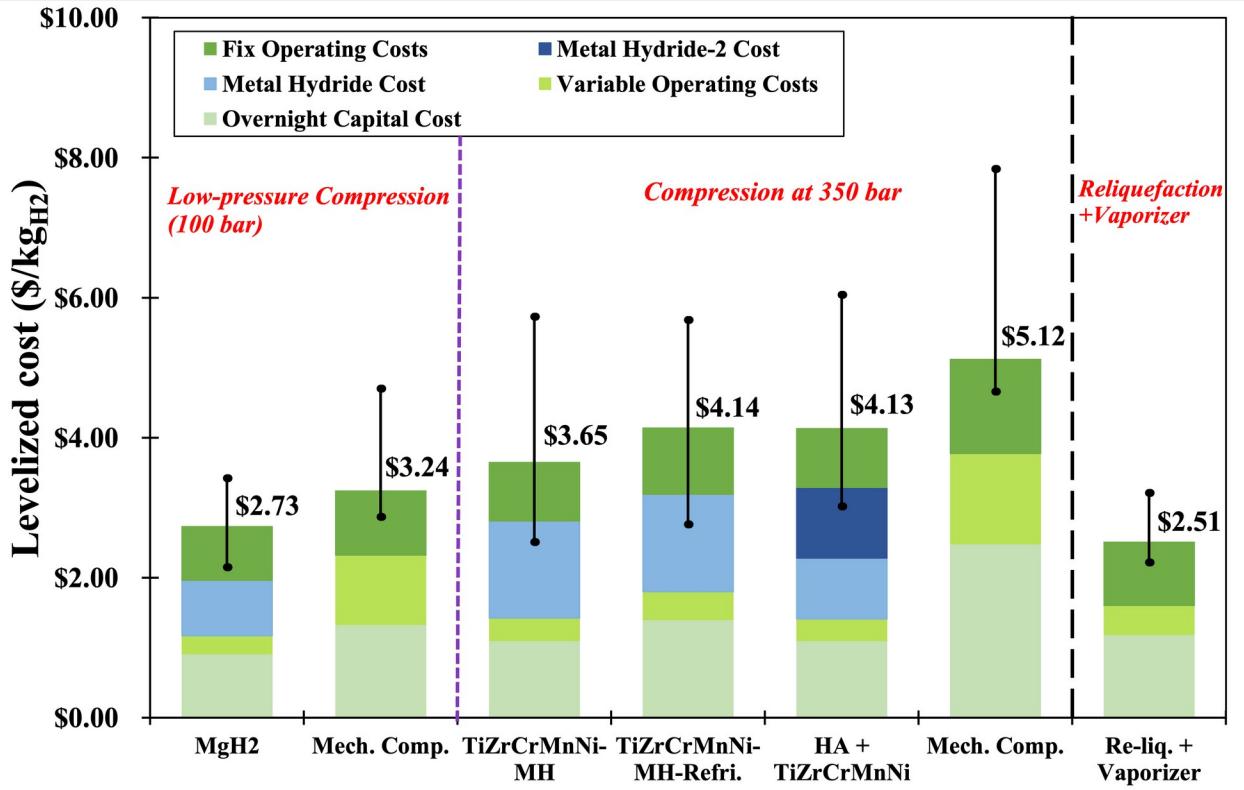


Figure 4. LCOH for low-pressure compression pathways: including mechanical and MgH_2 compression at 100 bar; MH compression, mechanical compression, and re-liquefaction-vaporization system at 350 bar. Note re-liquefaction-vaporization system at 100 bar was estimated at $2.22 /kg-H2 but is not shown.

Decomposing the levelized cost into its overnight capital cost (OCC), fixed operating cost (FOC), and variable operating cost (VOC) components under the same combined uncertainty (**Figure 5c–5h**) shows the robustness of the cost ranking and its dependence on each primary parameter. For both OCC and FOC (**Figure 5c–5f**), annual throughput is overwhelmingly dominant ($\rho \approx -0.86$ for OCC and −0.97 to −0.99 for FOC across all three systems); because throughput and the other site-level drivers are shared across pathways, the capital- and fixed-cost ordering is essentially deterministic, with the MH system giving (almost coinciding with the re-liquefaction-vaporization in most trials) the lowest OCC and mechanical compression the highest in >60% of the trials. The variable operating cost (**Figure 5g–5h**) separates the systems along technology-specific drivers: electricity price for mechanical compression ($\rho = +0.67$), hydride cycle life and material cost for the MH system ($\rho = -0.84$ and +0.45), and helium price for re-liquefaction-vaporization ($\rho =$

+0.82). Additionally, the re-liquefaction-vaporization VOC is both the lowest and the tightest of the three (mean ≈ \$0.43/kg-H_2). This is because of the lower energy demand of liquid-phase pumping and the complete avoidance of hydride cycling, and it is this advantage over VOC that ultimately makes the re-liquefaction-vaporization pathway most cost-effective even when capital and fixed costs are nearly tied with the MH system. These component-level trends mirror the deterministic CAPEX–OPEX breakdowns in Section 3.5, confirming that mechanical compression is penalized by high capital together with electricity- and cooling-dominated variable operating costs, the MH system by material-driven variable and thermal-cycling costs, and the re-liquefaction-vaporization system benefits from uniformly low capital, fixed, and variable costs, making it the most cost-advantageous and economically scalable BOH compression pathway.

When considering the potential of technologies to handle variations in CF, we find that the re-liquefaction–vaporization pathway can tolerate intermittent operation without large efficiency penalties by first re-liquefying BOH into the liquid phase and subsequently decoupling pressure rise through liquid pumping and vaporization. Cryogenic liquid pumps and cold-box equipment operate under relatively steady thermal and mechanical conditions, leading to stable performance, lower mechanical wear, and reduced maintenance intensity compared with gas-phase compression. Where mechanical compression requires extensive piping and high-grade materials capable of handling cyclic mechanical stresses and high discharge temperatures, the re-liquefaction–vaporization system operates primarily within the liquid phase, where the required compression work is an order of magnitude lower due to hydrogen's higher density and incompressibility. As a result, both the CAPEX and variable OPEX costs are reduced by approximately 50% and 66%, respectively, compared to mechanical compression at 350 bar discharge. Re-liquefaction-vaporization balances moderate CAPEX with much lower operating costs.

The re-liquefaction–vaporization system model also demonstrates cost superiority across all pressures evaluated. At 100 bar, re-liquefaction-vaporization still maintains the lowest LCOH of \$2.22 /kg-H_2. From a process standpoint, MH compressors can handle intermittent operation and would benefit from any available on-site waste heat to offset the thermal energy requirements for dehydrogenation and thereby reducing the operational cost. MH-based compression offers distinct advantages over mechanical compression for low-to-moderate pressure applications (< 350 bar),

where the endothermic desorption process can be driven by low-grade or waste heat with high-purity hydrogen delivery [24,72]. Mechanical compression is the least economical due to its high capital and energy burden, with significant spread in Overnight Capital Costs (**Figure S3**). Though mechanical compression is mature, high capital investment, electricity, and cooling water demand, and maintenance costs, make them less favorable at small-scale operations. At the same time, due to the uncertainty in MH performance, there are a number of scenarios where mechanical compression will be cost comparable with MH, as discussed in the following section.

To test whether the technology ranking survives simultaneously unfavorable assumptions, we consider the re-liquefaction-vaporization pathway under its combined worst case (80% re-liquefaction efficiency, operating lifetime of 20 years, and lower capacity factor (~750 tonnes BOH capture annually)). Under these combined conditions, the re-liquefaction-vaporization LCOH becomes closest (3.68 \$/kg-H_2) to the base case MH compression (3.64 \$/kg-H_2), so the ranking (re-liquefaction ≤ MH < mechanical) is still preserved. MH becomes competitive only under simultaneously favorable hydride cost and cycle life combined with available waste heat, consistent with **Figure S4e.**

Venting BOH constitutes a direct loss of recoverable product value, which can instead be monetized by deploying such BOH capture and compression systems, underscoring the relevance of this study for industries experiencing significant boil-off losses. Real-market benchmarks are provided in **Figure 6**, including average LH_2 delivery prices in California, USA (~\$10.5/kg) in 2024 [73], and projected LH_2 delivery prices in Rotterdam (Netherlands), and Japan from Norway [74], not including dispensing costs. For the base case of 5 tpd BOH stream, if the recovered hydrogen is used internally at 0 \$/kg (i.e. no resale), just recovering the purchased LH2 product would yield a payback period <10 years in all three: mechanical, MH compression, and re-liquefaction-vaporization. Both the MH compression and re-liquefaction-vaporization exhibit consistently lower payback periods compared to mechanical compression across the entire hydrogen selling price range. At LH_2 delivery prices of \$5-30/kg, MH compression achieves payback periods of 5 to 0.6 years, only marginally higher than re-liquefaction–vaporization system (3.5 to 0.5 years). For applications that receive cheaper LH_2, both the MH compression and re-liquefaction–vaporization offer a more economically attractive route for BOH utilization than mechanical compression. We

note that including dispensing/refueling costs would only shorten the payback periods, so the reported delivered LH_2 cost values are a conservative lower bound relative to a conventional refueling station.

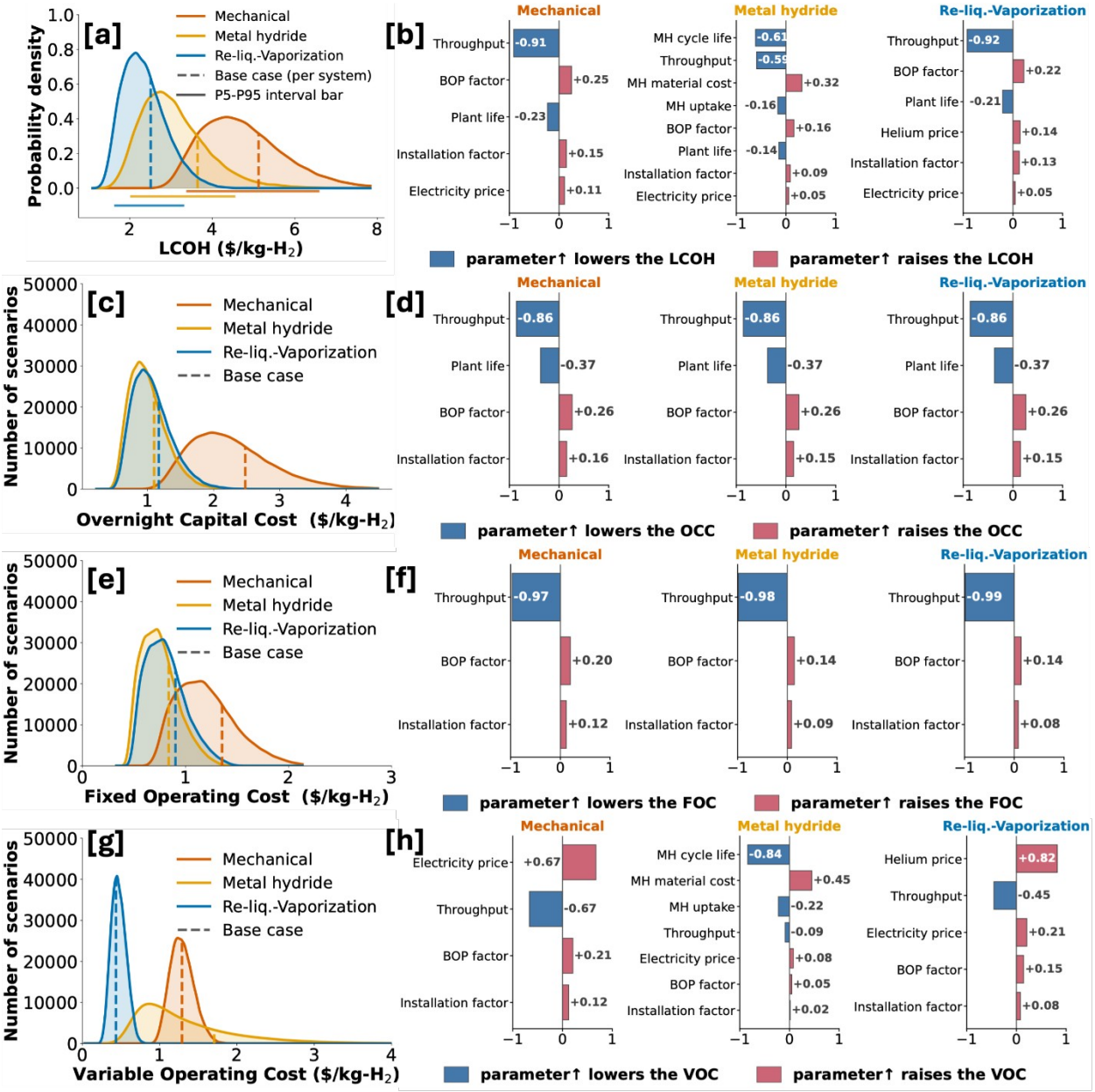


Figure 5. Combined probabilistic uncertainty analysis of BOH compression at 350 bar. (a) LCOH probability densities for the three pathways with base case markers and P5–P95 intervals. (b) Global (Spearman rank-correlation) sensitivity of LCOH to each parameter for each system. (c, e, g) Distributions of the overnight capital cost (OCC), fixed operating cost (FOC), and variable operating cost (VOC), in $/kg-$H_2$, across the 50,000 scenarios, with (d, f, h) the corresponding rank-correlation sensitivities. Blue bars denote parameters whose increase lowers the $/kg-$H_2$ BOH compression cost; red bars denote parameters

whose increase raises it. Plant-level drivers (annual throughput, plant life, installation and BOP factors, electricity price) are sampled once per trial and shared across pathways, whereas system-specific drivers (hydride material cost, cycle life, and uptake; helium price) are sampled independently.

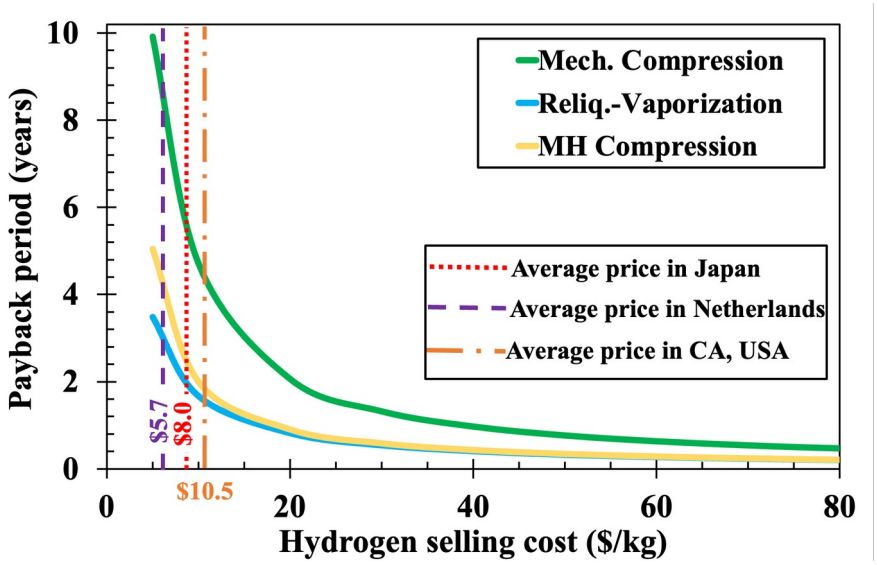


Figure 6. Payback period for hydrogen compression at 350 bar when only considering the direct lost value of the LH_2 in all three different pathways mentioned in this study. Example prices are for delivered liquid H_2, not the dispensing fuel price [73,74].

3.5 Opportunities for Cost reduction: When considering opportunities for TPC and LCOH reductions, the cryogenic and mechanical systems hold an advantage in that cost reduction is readily achievable in the near term with adjustments to facility design and plant operation (**Figure 7**). At the same time, these cost reductions are fairly well bound, whereas the potential for a system design or material breakthrough in MH research to disrupt costs is feasible. In particular, the limited availability of reliable MH desorption-kinetic data, introduces large uncertainties in cycle time, thermal duty, and long-term degradation rates, making it less predictable than mature and established mechanical compression systems [22,58]. The non-hybrid MH compression (using $Ti_{1.6}Zr_{0.4}CrMnFeNi$) reduces capital intensity substantially (TPC $8–$18M, **Figure 7c**) and can achieve much lower LCOH ($4.35–$2.27 /kg-H_2), but its performance is highly sensitive to hydride cycling life, purchasing cost, regeneration heat, MH's hydrogen storage capacity, and operator requirements, reflecting intrinsic material-driven operational uncertainty.

Notably, a number of deployment scenarios lead to the same LCOH for mechanical and MH compression. For example: (i) when MH cost exceeds ~$76 /kg with <950–1000 cycles before complete replacements and CF drops below 33% (~600 tpy BOH capture capacity), (ii) when the BOH compression efficiency of MH system falls under 70% meaning only <70% of captured BOH gets absorbed in MH beds, (iii) when mechanical compression system operate at very high CF (>90% or >1600 tpy annual capacity), or (iv) when BOP costs are relatively low (<30% of major equipment expenses).

As MH-based systems are tied to material cost and properties with greater uncertainty than the two other mechanical systems explored in this study, we present a scenario analysis to evaluate the impact of material-level advances on overall performance (**Figure S4**). Predictably, increasing MH hydrogen uptake to 2.0 wt.% reduces the required upfront and replacement quantities of MH and associated energy costs (**Figure S4a**). Extending the MH cycle life from 1,000 to 5,000 cycles does not affect energy costs, as we do not model degradation effects over time, but it does drive LCOH down to $2.76/kg, making cycle stability one of the most powerful cost levers in the system. As noted in previous TEA of MH-based systems, material price can quickly counter the economic viability and cost benefits for the MH-compression system (**Figure S4b**) [45]. When these factors are compared in the combined panel, we find that the high MH cost (50 $/kg) and low hydrogen capture capacity (1.2 wt.%) yields the maximum levelized cost of $4.54/kg-$H_2$, whereas favorable conditions such as high cycle life (5000 cycles), higher uptake (≥1.75 wt.%), low MH purchasing cost (25 $/kg), and higher BOH throughput (8 tpd) bring the LCOH drastically down to about $2.51 /kg-$H_2$, showcasing the economic spectrum of MH compression system. It is to be noted that at these optimized conditions, the LCOH of the $Ti_{1.6}Zr_{0.4}$CrMnFeNi-based MH compression system becomes equal to the base case re-liquefaction-vaporization system.

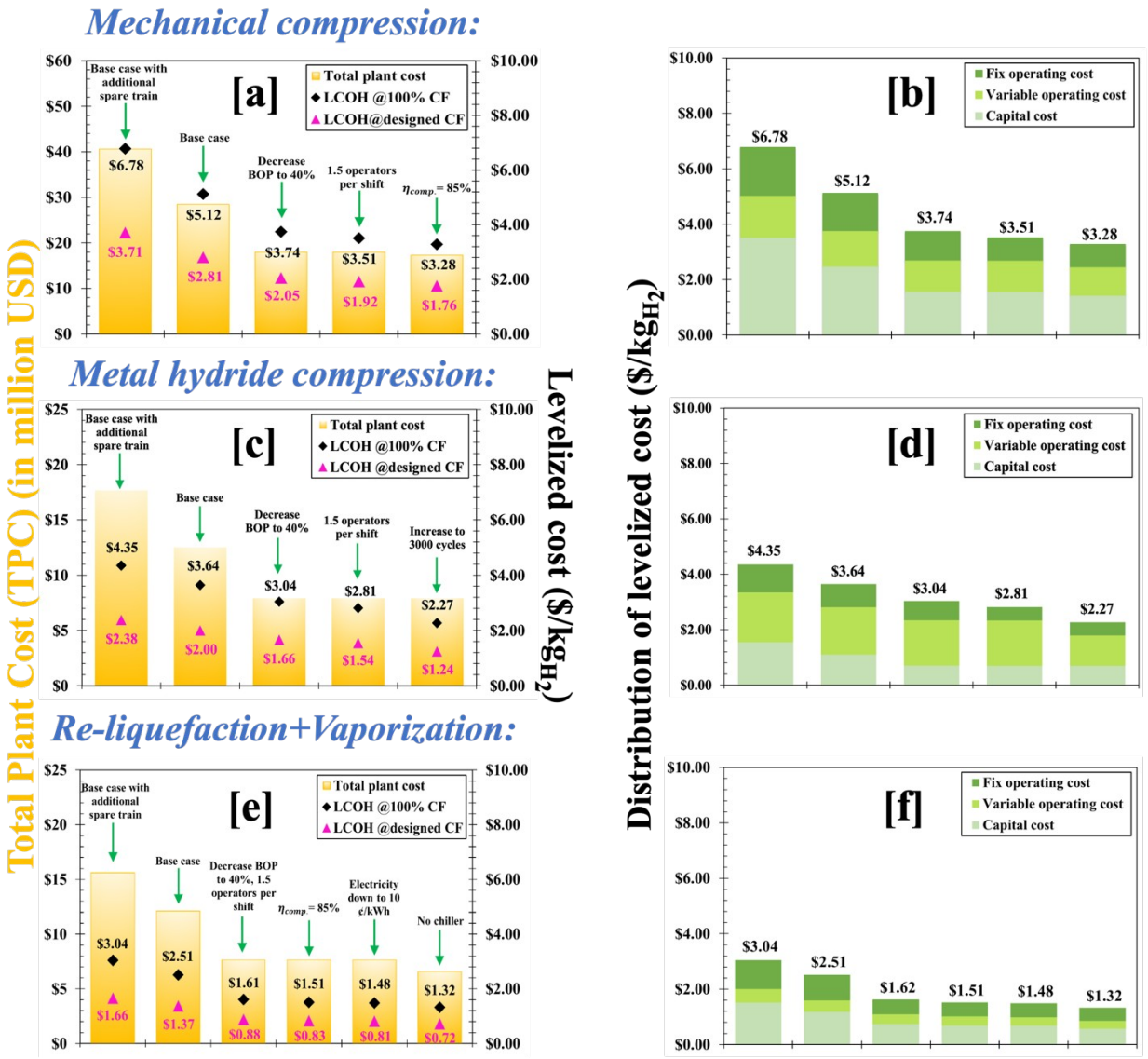


Figure 7. Total plant cost (TPC) and levelized cost of hydrogen (LCOH) sensitivity analysis for three BOH recovery-compression pathways—(a, b) mechanical compression, (c, d) non-hybrid $Ti_{1.6}Zr_{0.4}CrMnFeNi$-based MH compression, and (e, f) re-liquefaction-vaporization. Panels (a), (c), and (e) illustrate the sequential and cumulative evolution of TPC and corresponding LCOH under most critical and dominating design, operational, and economic scenarios, including the number of spare trains, reduced operator count and utility cost per unit, higher efficiency, lower MH cost or cycle-life adjustments, and reduced BOP for each system. Panels (b), (d), and (f) show the associated cost breakdowns into capital cost, fixed operating cost, and variable operating cost for each scenario.

3.6 Comparison of BOH compression at 700 bar: A comparison of energy and cost performance for 700-bar BOH compression systems reveals a similar pattern observed at 350 bar, but the magnitude of differences becomes more pronounced at higher discharge pressure. **Table 2** summarizes the key energy and techno-economic metrices for the BOH capture pathways considered in this study; details on the LCOH breakdowns and SEC are provided in the **ESI** for the 700 bar systems (**Figure S5**). Mechanical compression remains the most expensive BOH compression pathway, with an LCOH of \$6.37/kg-H_2 at 700 bar, largely driven by CAPEX (49%), similar to the lower pressure systems (**Figure 8**). This reflects a sharp rise in compressor size and cooling requirements for >600 bar multistage compressors, confirming that mechanical systems scale poorly with increasing compression pressure due to higher major equipment expenses at larger discharge pressures, higher flow of cooling water requirement, and correspondingly increased duty of intercoolers.

In contrast, non-hybrid MH-compression achieves an LCOH of \$3.94/kg-H_2 at 700 bar and again shows a cost advantage over mechanical systems (~38% lower LCOH), due to the elimination of expensive compressor hardware, thermally driven desorption, and a much smaller CAPEX (~31% of overall LCOH). We find that the desorption plateau pressure of the combination of $Ti_{1.6}Zr_{0.4}$CrMnFeNi (from 2-30 bar) and $Ti_{1.8}Zr_{0.2}$CrMnFeNi (from 30-700 bar) MH enables reaching 700 bar in only two stages of compression; however, the mechanical system requires an additional compression stage, which increases the LCOH by ~\$1.2 /kg-H_2. However, for the 700 bar case, as the thermodynamics of $Ti_{1.6}Zr_{0.4}$CrMnFeNi do not permit hydrogen desorption at 700 bar below 120 °C, therefore, another low-stability alloy from the same $Ti_{2-z}Zr_z$CrMnFeNi family ($Ti_{1.8}Zr_{0.2}$CrMnFeNi) is applied as it exhibits a higher plateau pressure, enabling hydrogen desorption at nearly ~80 °C at 700 bar [25]. At 700 bar, installed CAPEX for MH beds increases to 52%, reflecting the need for high-pressure bed design with $Ti_{1.8}Zr_{0.2}$CrMnFeNi for the 2nd stage compression. In comparison, for the MgH_2 system (100 bar), MH beds and initial fill of MgH_2 contribute to 47% and 12% of installed CAPEX. For the 350-bar base case ($Ti_{1.6}Zr_{0.4}$CrMnFeNi MH), MH beds contribute 43%, and the MH alloy fill contributes 19%, but in the hybrid case, the material cost is split between $Ti_{1.6}Zr_{0.4}$CrMnFeNi and Hydralloy at 10% and 11%, respectively. The

refrigeration-integrated MH compression system introduces additional refrigeration and heat exchanger costs, contributing to 10% and 7% of total installed CAPEX, respectively, which explains why LCOH for this is higher compared to the non-refrigerated base case.

The re-liquefaction-vaporization pathway LCOH for the 700 bar case only increases by 10% from \$2.51/kg-H_2 at 350 bar to \$2.75/kg-H_2 at 700 bar, mostly resulting from an increase in CAPEX due to an additional cryo-pumping stage. Importantly, the small jump in LCOH from 350 bar to 700 bar reflects the nearly linear $\Delta P/\rho$ scaling of pump power requirement. This system attains nearly 56% and 30% lower LCOH compared to mechanical and MH compression systems, respectively. When compared with mechanical compression at 700 bar, the re-liquefaction–vaporization system retains a ~56-60% reduction of the CAPEX-OPEX contribution in LCOH, confirming that this system's cost competitiveness becomes even more pronounced at higher pressures compared to the other BOH recovery strategies. In the cryogenic re-liquefaction-vaporization case, cryopumps and vaporizers contribute 13-18% of the total installed CAPEX cost for both 350 and 700 bar, while compressors account for 27-30%, respectively. The remaining cost is shared among the turbomachinery, balance of plants (piping, electrical, instrumentation, and site development), refrigeration (~8%), and the *ortho-para* hydrogen conversion reactor (only 3%). **Figure 8** establishes the previous observations that installed capital cost reduction for mechanical systems requires compressor stages and cooling-load reduction, and for MH compression, it demands optimized thermal management and refrigeration load reduction.

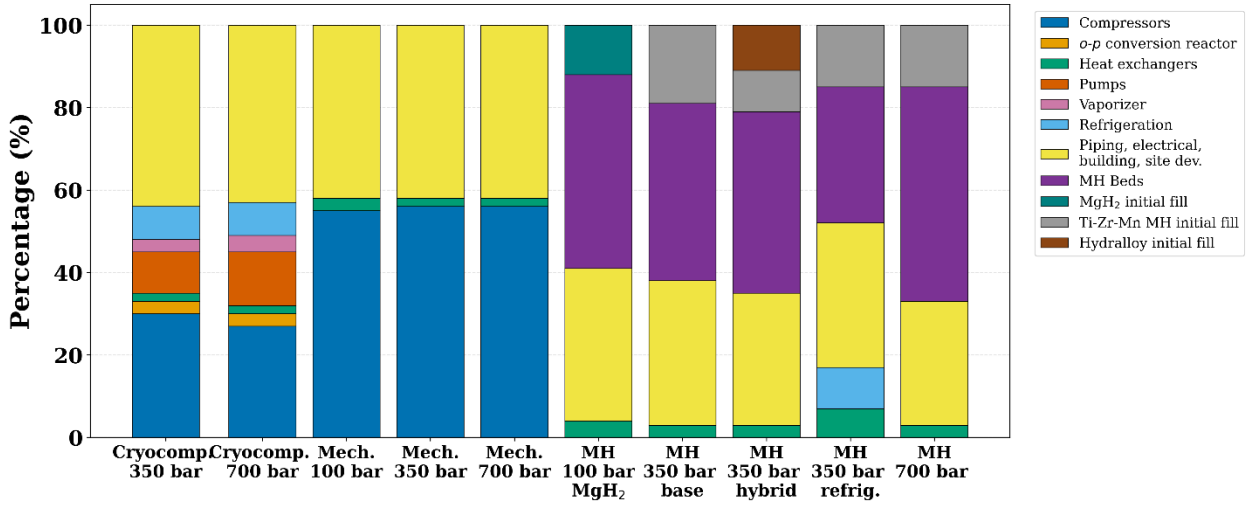


Figure 8. Breakdown of the total installed capital cost (normalized to 100%) of all equipment for three different BOH capture-compression technologies at different operating pressures.

Pathway	Pressure (bar)	LCOH ($/kg-$H_2$)	SEC (kWh/kg-H_2)	TPC	CAPEX contribution	Dominant cost driver
Mechanical compression	100	$3.24	2.57 (e)	$15.1M	~41%	CAPEX + cooling
	350	$5.12	3.21 (e)	$28.5M	~48%	CAPEX + cooling water
	700	$6.37	3.67 (e)	$35.9M	~49%	CAPEX + intercooler
$Ti_{1.6}Zr_{0.4}CrMnFeNi$ (non-hybrid, no refrig.)	350	$3.65	6.42 (th)	$12.5M	~30%	MH material cost
$Ti_{1.6}Zr_{0.4}CrMnFeNi$ + $Ti_{1.8}Zr_{0.2}CrMnFeNi$ (no refrig.)	700	$3.94	9.03 (th)	$14.0M	~32%	MH material + cycling
$Ti_{1.6}Zr_{0.4}CrMnFeNi$ + Hydralloy (hybrid, no refrig.)	350	$4.13	7.07 (th)	$12.5M.	~27%	MH material, Vanadium cost in Hydralloy
MgH_2	100	$2.73	10.42 (th)	$10.3M	~33%	Cycle life + replacement
Re-liquefaction-vaporization	100	$2.22	0.62 (e)	$10.3M	~45%	Cold-box + cryo CAPEX
	350	$2.51	0.95 (e)	$12.1M	~47%	Cold-box + cryo-pump
	700	$2.75	1.48 (e)	$13.6M	~48%	Additional cryo-pump stage

Table 2. Summary of different BOH capture pathways and corresponding operating pressures, energy, and cost ranges. In case of SEC, kWh(e)/kg-H_2 and kWh(th)/kg-H_2 refers to the electrical, and thermal energy requirements, respectively.

Conclusion: This study provides a broad techno-economic comparison of three compression pathways using mechanical, metal-hydride, and re-liquefaction–vaporization-based compression for boil-off hydrogen recovery for different low- to high-discharge pressure ranges up to 700 bar. The main findings are summarized below:

a. Mechanical Compression

- The technologically mature mechanical compression consistently comes out to be the most capital- and energy-intensive option, making it economically feasible and cost-competitive only when the system is operating at a high capacity factor (>60-75%) and larger annual BOH throughput.
- Mechanical compression becomes increasingly uneconomical at high discharge pressures and low capacity factors.

b. Metal-hydride (MH) Compression

- MH compression systems having cheaper thermally driven compressors offer significant advantages for this 5 tpd scale application.
- For the 350-bar compression case, the non-hybrid non-refrigeration loop MH systems achieve 25–40% lower LCOH than mechanical compressors, and even further reductions are possible under favorable material cost and cycling conditions.
- Non-hybrid non-refrigeration loop MH-based compression helps in reducing the overall CAPEX burdens and offers substantial technological and cost advantages at intermediate scales.
- Across the MH scenarios analyzed here, the non-hybrid, non-refrigerated $Ti_{1.6}Zr_{0.4}CrMnFeNi$-based MH compression system consistently achieves the lowest LCOH for 350 bar compression, since it minimizes system complexity by avoiding additional capital and fixed operating costs associated with integrating a refrigeration loop.
- On the other hand, hybrid MH systems involving Hydralloy incur higher LCOH due to much more expensive hydride costs, lower effective hydrogen desorption rate, and higher desorption enthalpy, compared to the non-hybrid MH system.

These indicate that, at the designed scale and while compressing hydrogen to 350 bar, the simplified heat-integrated single-material ($Ti_{1.6}Zr_{0.4}CrMnFeNi$) MH architecture showcases the most favorable balance between thermodynamic performance and system-level economics.

c. Re-liquefaction-vaporization

- The re-liquefaction–vaporization pathway consistently delivers the lowest LCOH across all pressures, enabled by liquid-phase pressurization that requires considerably less work than gas-phase compression.
- This architecture achieves ~50–66% reductions in the contribution of CAPEX and OPEX in LCOH relative to mechanical compression and maintains cost competitiveness even compared to optimized MH systems for the 350 bar systems.
- The LCOH goes down by ~12% when the discharge pressure is set at 100 bar from 350 bar, and increases by ~10% when setting the discharge pressure from 350 to 700 bar due to the favorable $\Delta P/\rho$ scaling of pump power, maintaining its technology advantage.

d. Considerations and limitations for MH systems

- The economics of this material-based system are promising; however, the competitive advantage over cryogenic-based compression depends on the hydride material properties, including reversible hydrogen storage capacity, MH purchasing cost, charging-discharging cycles before replenishment, and regeneration heat. We note that the lack of reliable kinetic data during thousands of hydrogen desorption cycles, limits the cost prediction accuracy needed during large-scale real-world deployments.
- When considering locations with potentially limited space, such as airports, system layout, modularity, and scalability may play a strong role in technology viability. Unlike mechanical systems that typically rely on variable-speed compressors and external cooling loops, MH systems benefit from passive thermal cycling and modular designs that can be tailored to variable flow rates and pressure targets. The compactness of MH beds, their cycling life, and material replacement frequency also influence long-term performance and economics.

- Integration of renewable or waste heat sources—such as from nearby electrolyzers or industrial processes—can significantly improve energy efficiency and reduce operational costs. However, the capital-intensive nature of high-purity MHs and the requirement for robust heat exchangers necessitate a rigorous TEA assessment to benchmark against mature mechanical systems.

Overall, the cross-system comparison confirms that the re-liquefaction–vaporization configuration emerges as the most cost-effective and scalable pathway for BOH recovery, especially in facilities with existing cryogenic infrastructure. Notably, all systems hold advantages over direct venting of BOH at higher hydrogen prices. Collectively, these insights provide a systematic basis for selecting BOH recovery technologies in stationary storage of liquid hydrogen, transfer events, and fueling infrastructures, highlighting the potential of liquid-phase pressurization and materials-based compression strategies to transform hydrogen delivery systems and minimize energy loss by venting out the BOH. The 700 bar comparison clearly establishes the fundamental physics governing all three pathways similar to the 350 bar case but at a bigger scale: mechanical compression becomes increasingly uneconomical at high pressure, MH compression performs better but highly sensitive to material cost and cycling durability, and the re-liquefaction-vaporization system delivers both low CAPEX and OPEX through liquid-phase pressurization using additional cryo-pumping stages and better thermal management. When these are combined with the 350 bar TEA results, we can see that the economic gap widens with high-pressure discharge, making the re-liquefaction-vaporization configuration the more scalable and cost-efficient system for high-pressure BOH recovery.

Acknowledgements:

The authors gratefully acknowledge support from the U.S. Department of Energy (DOE) for the funding of this project through grant EE0011104 from the U.S. DOE, Office of Energy Efficiency and Renewable Energy, Hydrogen Fuel Cell Technologies Office in Fiscal Year 2025 under Contract No. DE-AC02-05CH11231 with the Lawrence Berkeley National Laboratory, and Contract No. DE-AC36-08GO28308 for National Laboratory of the Rockies. Sandia National Laboratories is a multi-mission laboratory managed and operated by National Technology & Engineering Solutions of Sandia, LLC (NTESS), a wholly owned subsidiary of Honeywell International Inc., for the U.S. DOE's National Nuclear Security Administration (DOE/NNSA) under contract DE-NA0003525. This written work was authored by an employee of NTESS. Any subjective views or opinions that might be expressed in the written work do not necessarily represent the views of the U.S. Government. The publisher acknowledges that the U.S. Government retains a non-exclusive, paid-up, irrevocable, world-wide license to publish or reproduce the published form of this written work or allow others to do so, for U.S. Government purposes. The DOE will provide public access to results of federally sponsored research in accordance with the DOE Public Access Plan. The authors thank Stoke Space Technologies and Airbus for their insights on aerospace and aviation sector market viability. The authors thank Dr. Zeric Hulvey for his support and guidance.

References:

1. Gil-Esmendia, A., Flores, R. J. & Brouwer, J. Modeling and improving liquid hydrogen transfer processes. *Appl. Energy* **390**, 125779 (2025).
2. Morales-Ospino, R., Celzard, A. & Fierro, V. Strategies to recover and minimize boil-off losses during liquid hydrogen storage. *Renewable and Sustainable Energy Reviews* **182**, 113360 (2023).
3. Hossain Bhuiyan, M. M. & Siddique, Z. Hydrogen as an alternative fuel: A comprehensive review of challenges and opportunities in production, storage, and transportation. *Int. J. Hydrogen Energy* **102**, 1026–1044 (2025).
4. Aydezott, J. C. & Spuckzer, C. M. Venting of liquid hydrogen tankage. Preprint at (1969).
5. Souers, P. C., Briggs, C. K., Pyper, J. W., Tsugawa, R. T. & California Univ., L. (USA). L. L. L. Hydrogen vapor pressures from 4 to 30 K: a review. Preprint at https://inis.iaea.org/records/2793x-d5q31 (1977).
6. Al Ghafri, S. Z. *et al.* Hydrogen liquefaction: a review of the fundamental physics, engineering practice and future opportunities. *Energy Environ. Sci.* **15**, 2690–2731 (2022).
7. Trapani, D., Marocco, P., Gandiglio, M. & Santarelli, M. Hydrogen leakages across the supply chain: Current estimates and future scenarios. *Int. J. Hydrogen Energy* **145**, 1084–1095 (2025).
8. Popovich, N. Hydrogen Station Compression, Storage, and Dispensing Technical Status and Costs: Systems Integration. Preprint at https://research-hub.nrel.gov/en/publications/hydrogen-station-compression-storage-and-dispensing-technical-sta/ (2014).
9. Hua, T. Q. *et al.* Technical assessment of compressed hydrogen storage tank systems for automotive applications. *Int. J. Hydrogen Energy* **36**, 3037–3049 (2011).
10. Mohammadi, A. *et al.* High-entropy hydrides for fast and reversible hydrogen storage at room temperature: Binding-energy engineering via first-principles calculations and experiments. *Acta Mater.* **236**, 118117 (2022).
11. Charbonnier, V., Enoki, H., Asano, K., Kim, H. & Sakaki, K. Improvement of hydrogenation sorption properties of Ti0.90V0.30Mn1.00Ni0.80 for ultra-high pressure metal-hydride compressor. *Int. J. Hydrogen Energy* **47**, 32252–32261 (2022).
12. Li, R. *et al.* Development of Ti-Zr-Mn based AB2 type metal hydrides alloys for an 865 bar two-stage hydrogen compressor. *Int. J. Hydrogen Energy* **72**, 687–693 (2024).
13. Hou, Z. *et al.* Hydrogen storage and stability of rare earth-doped TiFe alloys under extensive cycling. *Int. J. Hydrogen Energy* **136**, 469–476 (2025).
14. Korol, A. A. *et al.* Hydrogen Storage in TiFe-Based Alloys Doped with Cr and S: Thermodynamic and Structural Peculiarities. *Energy & Fuels* **39**, 24396–24403 (2025).
15. Sui, Y. *et al.* Recent progress of nanotechnology in enhancing hydrogen storage performance of magnesium-based materials: A review. *Int. J. Hydrogen Energy* **47**, 30546–30566 (2022).

16. Li, Q. *et al.* Thermodynamics and kinetics of hydriding and dehydriding reactions in Mg-based hydrogen storage materials. *Journal of Magnesium and Alloys* **9**, 1922–1941 (2021).

17. Wang, X., Liu, H. & Li, H. A 70 MPa hydrogen-compression system using metal hydrides. *Int. J. Hydrogen Energy* **36**, 9079–9085 (2011).

18. Yartys, V. A. *et al.* Metal hydride hydrogen compression: recent advances and future prospects. *Applied Physics A 2016 122:4* **122**, 415- (2016).

19. Scarpati, G., Frasci, E., Di Ilio, G. & Jannelli, E. A comprehensive review on metal hydrides-based hydrogen storage systems for mobile applications. *J. Energy Storage* **102**, 113934 (2024).

20. Yartys, V. A. & Lototskyy, M. V. Laves type intermetallic compounds as hydrogen storage materials: A review. *J. Alloys Compd.* **916**, 165219 (2022).

21. Tarasov, B. P., Bocharnikov, M. S., Yanenko, Y. B., Fursikov, P. V. & Lototskyy, M. V. Cycling stability of RNi5 (R = La, La+Ce) hydrides during the operation of metal hydride hydrogen compressor. *Int. J. Hydrogen Energy* **43**, 4415–4427 (2018).

22. Khan, H. B. & Zhang, T. Metal hydride hydrogen storage risk assessment: A review. *J. Energy Storage* **129**, 117273 (2025).

23. Yartys, V. A. *et al.* Magnesium based materials for hydrogen based energy storage: Past, present and future. *Int. J. Hydrogen Energy* **44**, 7809–7859 (2019).

24. Bellosta von Colbe, J. *et al.* Application of hydrides in hydrogen storage and compression: Achievements, outlook and perspectives. *Int. J. Hydrogen Energy* **44**, 7780–7808 (2019).

25. Way, L. *et al.* Efficiently predicting pressure-composition-temperature diagrams to discover low-stability metal hydrides. *J. Mater. Chem. A Mater.* **14**, 2967–2976 (2026).

26. Qiu, G., Wang, K., Zhu, S. & Qiu, L. Hydrogen refueling station synergistically driven by liquid hydrogen pump and thermal compression. *Int. J. Hydrogen Energy* **56**, 441–451 (2024).

27. Plachta, D. W., Johnson, W. L. & Feller, J. Cryogenic Boil-Off Reduction System Testing. Preprint at www.nasa.gov (2014).

28. Chen, D., Naticchioni, L., Khalaidovski, A. & Radebaugh, R. Cryocoolers: the state of the art and recent developments*. *Journal of Physics: Condensed Matter* **21**, 164219 (2009).

29. Product: Cryogenic Solutions. https://resources.plugpower.com/product-cryogenic-solutions.

30. Plug Power Inc. | Plug Delivers Several Portable Liquid Hydrogen Refuelers to Customers. https://www.ir.plugpower.com/press-releases/news-details/2024/Plug-Delivers-Several-Portable-Liquid-Hydrogen-Refuelers-to-Customers/default.aspx?_gl=1*14cwzj*_ga*MjA1MDgyMTI1NC4xNzY1MjM3NDM2*_ga_MWCMJHDG1R*czE3NjUyMzc0NDIkbzEkZzAkdDE3NjUyMzc0NDIkajYwJGwwJGgw.

31. AspenTech. Aspen Plus (Version 14.0). *Aspen Technology, Inc.* (2022).

32. Al-Malah, K. I. M. Aspen Plus®. *Aspen Plus*® https://doi.org/10.1002/9781119293644 (2016) doi:10.1002/9781119293644.

33. Al-Malah, K. I. M. Aspen Process Economic Analyzer (APEA). *Aspen Plus*® 523–564 (2016) doi:10.1002/9781119293644.ch17.

34. Banerjee, T., Bravo, J., Sarunac, N., D'Agostini, M. & Romero, C. Sustainable energy storage solutions for coal-fired power plants: A comparative study on the integration of liquid air energy storage and hydrogen energy storage systems. *Energy Convers. Manag.* **310**, 118473 (2024).

35. Yin, L. & Ju, Y. Process optimization and analysis of a novel hydrogen liquefaction cycle. *International Journal of Refrigeration* **110**, 219–230 (2020).

36. Ali, A. *et al.* A review on application of hydrogen in gas turbines with intercooler adjustments. *Results in Engineering* **22**, 101979 (2024).

37. Huot, J., Lu, Z.-H., Franco, A. & Giovannini, C. Hydrogen Gas Compression for Efficient Storage: Balancing Energy and Increasing Density. *Hydrogen 2024, Vol. 5, Pages 293-311* **5**, 293–311 (2024).

38. Luo, Q. H., Sun, B. G. & Tian, H. Y. The characteristic of polytropic coefficient of compression stroke in hydrogen internal combustion engine. *Int. J. Hydrogen Energy* **39**, 13787–13792 (2014).

39. Turton, R., Bailie, R. C., Whiting, W. B. & Shaeiwitz, J. A. *Analysis, Synthesis and Design of Chemical Processes*. *Technology & Engineering* (Pearson Education, 2008).

40. Lugo-Méndez, H. *et al.* Interstage Pressures of a Multistage Compressor with Intercooling. *Entropy 2021, Vol. 23,* **23**, (2021).

41. Bauer, A., Mayer, T., Semmel, M., Guerrero Morales, M. A. & Wind, J. Energetic evaluation of hydrogen refueling stations with liquid or gaseous stored hydrogen. *Int. J. Hydrogen Energy* **44**, 6795–6812 (2019).

42. Pohlmann, C., Röntzsch, L., Heubner, F., Weißgärber, T. & Kieback, B. Solid-state hydrogen storage in Hydralloy–graphite composites. *J. Power Sources* **231**, 97–105 (2013).

43. Kölbig, M., Bürger, I. & Linder, M. Thermal applications in vehicles using Hydralloy C5 in single and coupled metal hydride systems. *Appl. Energy* **287**, 116534 (2021).

44. Johnson, T. A. *et al.* Metal Hydride Compressor for High-Pressure (875 bar) Hydrogen Delivery. https://doi.org/10.2172/1898257 (2022) doi:10.2172/1898257.

45. Wang, X. *et al.* Technoeconomic Insights into Metal Hydrides for Stationary Hydrogen Storage. *Advanced Science* **12**, 2415736 (2025).

46. Theis, J. Quality Guidelines for Energy Systems Studies: Cost Estimation Methodology for NETL Assessments of Power Plant Performance. https://doi.org/10.2172/1567736 (2021) doi:10.2172/1567736.

47. Rosner, F. *et al.* Green steel: design and cost analysis of hydrogen-based direct iron reduction. *Energy Environ. Sci.* **16**, 4121–4134 (2023).

48. Schmitt, T. *et al.* Cost and Performance Baseline for Fossil Energy Plants Volume 1: Bituminous Coal and Natural Gas to Electricity. https://doi.org/10.2172/1893822 (2022) doi:10.2172/1893822.

49. Towler, G. & Sinnott, R. *Chemical Engineering Design | ScienceDirect*. (Butterworth-Heinemann, 2021).

50. Mignard, D. Correlating the chemical engineering plant cost index with macro-economic indicators. *Chemical Engineering Research and Design* **92**, 285–294 (2014).

51. The Chemical Engineering Plant Cost Index ® - Chemical Engineering. https://www.chemengonline.com/pci-home.

52. Woods, D. R. Rules of Thumb in Engineering Practice. *Rules of Thumb in Engineering Practice* 1–458 (2007) doi:10.1002/9783527611119.

53. Breunig, H. *et al.* Achieving gigawatt-scale green hydrogen production and seasonal storage at industrial locations across the U.S. *Nature Communications 2024 15:1* **15**, 9049- (2024).

54. Kramer, D. Helium prices surge to record levels as shortage continues. *Phys. Today* **76**, 18–20 (2023).

55. Falcão, B. da S. *et al.* Ortho- to para-hydrogen catalytic conversion kinetics. *Int. J. Hydrogen Energy* **62**, 345–351 (2024).

56. Weitzel, D. H., Loebenstein, W. V, Draper, J. W. & Park, O. E. Ortho-Para Catalysis In Liquid-Hydrogen Production I. *J. Res. Natl. Bur. Stand. (1934).* **60**, (1958).

57. Nandiyanto, A. B. D., Maulana, M. I., Raharjo, J., Sunarya, Y. & Minghat, A. D. Techno-economic analysis for the production of LaNi5 particles. *Communications in Science and Technology* **5**, 70–84 (2020).

58. Mehr, A. S., Phillips, A. D., Brandon, M. P., Pryce, M. T. & Carton, J. G. Recent challenges and development of technical and technoeconomic aspects for hydrogen storage, insights at different scales; A state of art review. *Int. J. Hydrogen Energy* **70**, 786–815 (2024).

59. Shamoushaki, M., Niknam, P. H., Talluri, L., Manfrida, G. & Fiaschi, D. Development of Cost Correlations for the Economic Assessment of Power Plant Equipment. *Energies 2021, Vol. 14, Page 2665* **14**, 2665 (2021).

60. Rustagi, N., Joseck, F. & Satyapal, S. *Current Status of Hydrogen Liquefaction Costs*. (2019).

61. BGR - Mineral Raw Materials - Price Monitor December 2019. https://web.archive.org/web/20200125021323/https://www.bgr.bund.de/DE/Themen/Min_rohstoffe/Produkte/Preisliste/pm_19_12.pdf.

62. China Other Minor Metals spot Price Chart Today - Shanghai Metals Market. https://archive.ph/20200203230442/https://price.metal.com/spots/Other-Minor-Metals/201211080001.

63. China Pig Iron spot Price Chart Today - Shanghai Metals Market. https://archive.ph/20200203202438/https://price.metal.com/spots/Pig-Iron/201808140002.

64. Peters, M. S., Timmerhaus, K. D. & West, R. E. *Plant Design and Economics for Chemical Engineers - Max S. Peters, Klaus D. Timmerhaus, Ronald Emmett West - Google Books*. (McGraw-Hill Education, 2003).

65. Danebergs, J. & Deledda, S. Can hydrogen storage in metal hydrides be economically competitive with compressed and liquid hydrogen storage? A techno-economical perspective for the maritime sector. *Int. J. Hydrogen Energy* **50**, 1040–1054 (2024).

66. Brennan, D. J. & Golonka, K. A. New Factors for Capital Cost Estimation in Evolving Process Designs. *Chemical Engineering Research and Design* **80**, 579–586 (2002).

67. Modi, P. & Aguey-Zinsou, K. F. Room Temperature Metal Hydrides for Stationary and Heat Storage Applications: A Review. *Front. Energy Res.* **9**, 616115 (2021).

68. Yang, C. C., Wang, C. C., Li, M. M. & Jiang, Q. A start of the renaissance for nickel metal hydride batteries: a hydrogen storage alloy series with an ultra-long cycle life. *J. Mater. Chem. A Mater.* **5**, 1145–1152 (2017).

69. Enblom, V. *et al.* A combined experimental and machine learning exploration of Ti2-xZrxMnCrFeNi high entropy Laves hydrides. *Materialia (Oxf).* **40**, 102414 (2025).

70. Bürger, I., Dieterich, M., Pohlmann, C., Röntzsch, L. & Linder, M. Standardized hydrogen storage module with high utilization factor based on metal hydride-graphite composites. *J. Power Sources* **342**, 970–979 (2017).

71. Morgan, S., How is primary energy defined and used? Library of Congress, *Energy & Natural Resources Reports*, R48270 (11/19/2024). https://www.congress.gov/crs-product/R48270?__cf_chl_tk=UpRFjaQqGLnQ.oyO85sdhpZBWAz79fLIiWm_lFtnOGs-1790761444-1.0.1.1-4_lB2K4z1uuRgvTvINvy44r8IxMv3nHM2HMVZJk28wQ

72. Klopčič, N., Grimmer, I., Winkler, F., Sartory, M. & Trattner, A. A review on metal hydride materials for hydrogen storage. *J. Energy Storage* **72**, 108456 (2023).

73. Ku, A. Y. *et al.* Driving towards competitive hydrogen dispensing cost for heavy-duty road transport: Quantifying and mitigating near-term operational penalties. *Int. J. Hydrogen Energy* **184**, 151781 (2025).

74. Andreassen, K., Buenger, U. H., Henriksen, N., Øyvann, A. & Ullmann, O. Large-scale production and transport of hydrogen from Norway to Europe and Japan: Value chain analysis and comparison of liquid hydrogen and ammonia as energy carriers. *Int. J. Hydrogen Energy* **45**, 32865–32883 (2020).